Optical and Quantum Electronics (2022) 54:714
https://doi.org/10.1007/s11082-022-04118-4

Theoretical study on spectral and optical properties of essential amino acids: a comparative study

Shradha Lakhera[1] · **Meenakshi Rana**[1] · **Kamal Devlal**[1]

Received: 28 April 2022 / Accepted: 16 August 2022

Abstract

In the present work, a theoretical study has been performed targeting essential amino acids (EAA) **Histidine**, **Isoleucine, Leucine, Lysine, Methionine, Phenylalanine, Threonine, Tryptophan, Valine**, and predicted their different physical and chemical properties by using computational techniques. Amino acids (AA), a fundamental structural unit of protein are amino and carboxyl-rich compounds having electrophilic and nucleophilic regions in them. The reactivity of AA was determined by computing molecular electrostatic potential (MEP) surfaces, counterplots, dipole moment, band gap, global reactivity parameters, and polarizability parameters. Spectral analysis (UV–Vis, Raman) helps in studying their electronic and vibrational properties. The polarizability and first-order hyperpolarizability parameters were also computed to detect the nonlinear optical (NLO) behavior of AA. The comparison done with reference NLO materials Urea, Phenyl urea, and 3-nitroaniline showed that **Phenylalanine** has higher hyperpolarizability and can better be used as a potent NLO material.

Graphical abstract

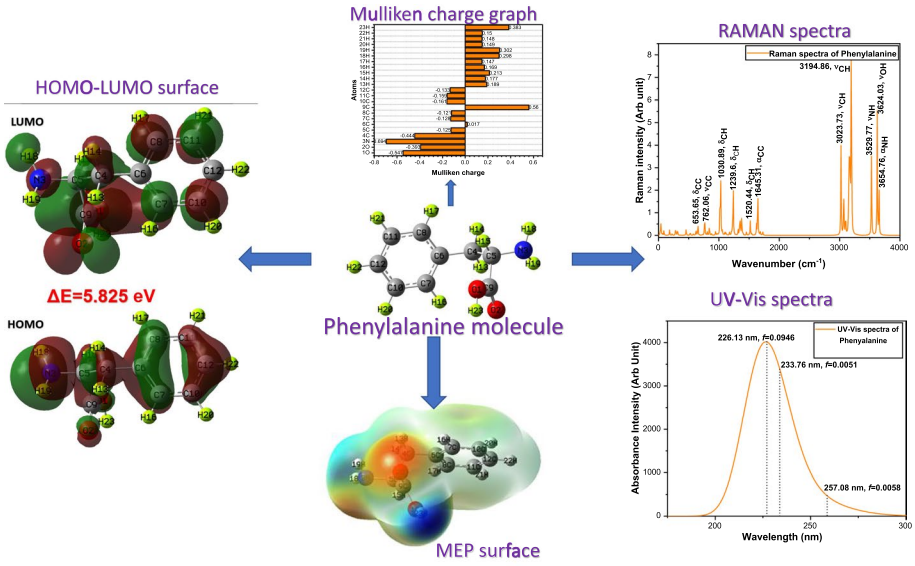

Extended author information available on the last page of the article

Keywords Essential amino acids · Optimization · Mulliken charges · Chemical reactivity · Spectral analysis

1 Introduction

Nonlinear optical (NLO) activity accounts for the polarization behavior of any material under the applied electric field (Oyeneyin et al. 2022). NLO properties deal with the displacement of the propagation characteristics of light (Ray 2010). When the phase, frequency, amplitude, polarization, etc. of the incident light changes under the applied electric field, the material possesses NLO behavior (Bairy et al. 2021). NLO is a very emergent topic in the current research world, exhibiting great diversity. It can be considered a multidisciplinary field of research as it has engineering and mechanical bias, and is a subject of physical sciences, and sometimes its applications can also be seen in chemical and biological science (Midgley et al. 2009; Lakhera et al. 2022a, b, c, d). In today's technology-dependent society, the need for efficient materials is increasing with every passing day. NLO materials have an extensive area of applications from uses in future integrated photonic technologies, telecommunications, sum, and difference frequency generation to microfabrication, optical rectification, frequency mixing wave generation, electro-optic modulation, frequency conversion, fluorescence imaging, etc. (Ullah et al. 2020; Buriahi et al. 2020; Cheng et al. 2019). NLO materials have been explored from various materials like molecular chromophores, polymers, semiconductors, etc., and also artificially designed such as lithium niobate ($LiNbO_3$) and potassium dihydrogen phosphate (KH_2PO_4) (Moroz and Maslovskaya 2021). Carbon is known to form different fascinating compounds. The basic reason is the sp^2 hybridization of carbon that gives rise to the immense quantity of delocalized π-electrons available for the ICT makes it highly reactive with different elements. Thus, the carbon compounds like fullerenes and carbon nanotubes have been an attractive field of research for researchers. The studies with the introduction of highly efficient NLO carbon compounds have been reported in the literature survey. Fullerenes like $C_{58}BN$ and $C_{60}Cl_{30}$ were reported to have 105.01×10^{-36} esu and 136.10×10^{-36} esu values of first-order hyperpolarizability (Muhammad et al. 2013). The carbon nanotubes have also been reported to have high third-order mean polarizability amplitudes like zigzag arranged nanotube 48.60×10^{-36} esu and an armchair arranged nanotube 43.52×10^{-36} esu (Muhammad et al. 2016, 2013). The amino acids (AA), fall in the category of carbon compounds. The organic compound-based NLO materials are gaining much attention and are preferred by most scientists worldwide because of their properties like high durability, high structural flexibility, high electronic susceptibility, short response time, easy availability, and synthesis. The innumerable stretchability and extensive response time make organic NLO materials more efficient than inorganic NLO materials (Naseema et al. 2020). Generally, the presence of π-electron conjugated moiety with electron donor and electron acceptor groups in organic molecules leads to remarkable NLO performance (Lee et al. 2021). Keeping this in mind, we have tried to detect the NLO behavior of AA. AA is the fundamental compound in protein formation. They consist of amino ($–NH_2$) and carboxyl (–COOH) functional groups. Nitrogen atoms present in the amino group constitute electron density to a greater extent. The higher the free electron pairs, the higher will be the availability of electrons for donation (Rana et al. 2019). The presence of the amino group also makes AA nucleophilic and carboxyl groups develop the electrophilic behavior. The oxygen atoms present in the carboxyl group are electronegative which draws electron cloud away from carbon making AA electrophilic (King et al. 2021). AA is generally divided into three main categories i.e., essentials (which cannot be synthesized by the body or

must be consumed), non-essentials (which are self-synthesized in the body), and conditional AA (which are not necessarily required generally except the illness or deficiency) (Then et al. 2020; Lopez and Mohiuddin 2022; Javier-Hila et al. 2021; Wang et al. 2021).

In the current study, we have considered nine essential amino acids (EAA) (**Histidine, Isoleucine, Leucine, Lysine, Methionine, Phenylalanine, Threonine, Tryptophan, and Valine**) (Table 1). This AA is synthesized into our body by the breakdown of the consumed protein and thus leads to the growth and development of muscles and immunity (Soares et al. 2020). They are available in plenty and consumed by external sources like meat, eggs, and poultry and can lead to wider applications in pharmacological sciences (Christophersen and Haug 2011).

Optimized structures for all nine EAA are presented in Table 1. The dipole moment and polarizability is the virtue by which the polarizing ability of any compound can be studied (Kuramochi et al. 2020). Mulliken charges and molecular electrostatic potential (MEP) surface have been done for all AA. Spectra like UV–Vis and Raman are also reported to check the spectral properties of the AA. The computed frontier molecular orbital (FMO) parameters are reported to justify the chemical reactivity of the compounds. Hyperpolarizability is the quantities by which the NLO behavior of any compound can be predicted (Lakhera et al. 2022a, b, c, d). The more the compound is polarizable, the more it will show NLO behavior (Nazrin et al. 2019). The calculations for the polarizability parameters are also carried out to understand the NLO responses of the compound.

2 Computational procedure and calculation

The structures of the EAA are downloaded from the online database "PubChem" (https://pubchem.ncbi.nlm.nih.gov/) (Table 1). All the computational calculations were carried out using Gaussian 09 software and the interpretation of the output is done with the help of the graphic user interface Gauss View 5.0 (Frisch et al. 2009; Becke 1993, 1997). Becke-3-Lee–Yang–Parr (B3) exchange function combined with (LYP) correlation is used for optimization (Dennington et al. 2007). The geometries of all the considered EAA are optimized using density functional theory (DFT) with the standard B3LYP/6-311G basis set. The optimized structure helps in obtaining the FMO energies. The rest of the parameters like ionization potential (*IP*), energy gap (ΔE), electron affinity (*EA*), chemical potential (*CP*), electronegativity (χ), softness (*S*), and hardness (η) are calculated with the help of these orbital energies. These parameters are calculated with the help of Koopman's equations given below (Koopmans 1934; Ojo et al. 2020; Oyeneyin et al. 2022):

$$IP = -E_{HOMO} \tag{1}$$

$$EA = -E_{LUMO} \tag{2}$$

$$CP = \frac{E_{HOMO} + E_{LUMO}}{2} \tag{3}$$

$$\chi = \frac{(IP + EA)}{2}, \tag{4}$$

Table 1 Optimized structures of EAA by standard B3LYP/6-311G basis set with PubChem IDs and chemical formulas

AA	PubChem ID	Chemical formula	Structure
Histidine	6274	$C_6H_9N_3O_2$	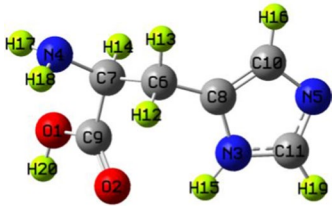
Isoleucine	6306	$C_6H_{13}NO_2$	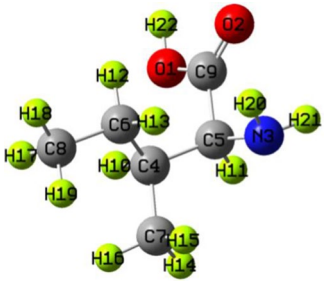
Leucine	6106	$C_6H_{13}NO_2$	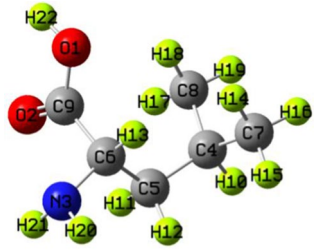
Lysine	5962	$C_6H_{14}N_2O_2$	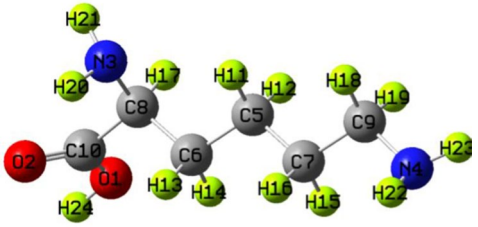
Methionine	6137	$C_5H_{11}NO_2S$	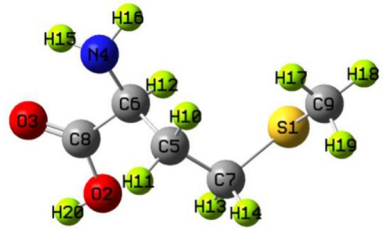

Table 1 (continued)

AA	PubChem ID	Chemical formula	Structure
Phenylalanine	6140	$C_9H_{11}NO_2$	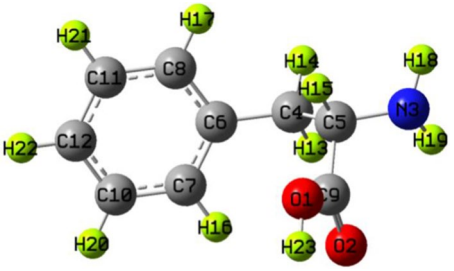
Threonine	6288	$C_4H_9NO_3$	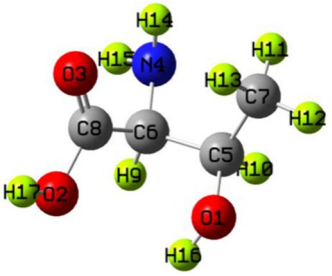
Tryptophan	6305	$C_{11}H_{12}N_2O_2$	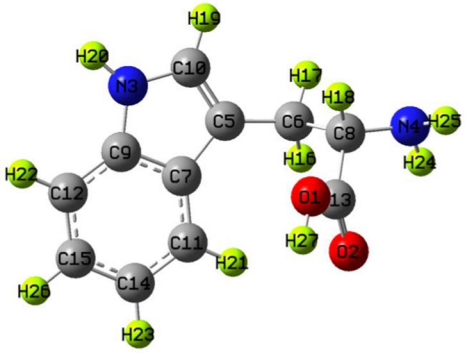
Valine	6287	$C_5H_{11}NO_2$	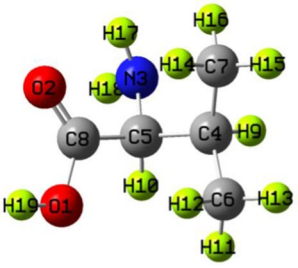

$$\eta = \frac{E_{LUMO} - E_{HOMO}}{2}, \; S = \frac{1}{\eta} \tag{5}$$

In Raman spectra analysis, Raman intensity is also calculated corresponding to high frequency modes. It was calculated by below given expression:

$$I = \frac{f(vo - vi)^4 \mathrm{Si}}{vi\left[1 - \exp\left(-\frac{hcvi}{\mathrm{kT}}\right)\right]} \tag{6}$$

where I refer to Raman intensity of the considered mode, f is a constant with value 10^{-12}, ν_o has value 9398.5 cm^{-1}. ν_i and S_i is the vibrational wavenumber and Raman activity of selected mode respectively. h is Planck constant with value 4.1357×10^{-15} eV K^{-1}, c is speed of light with value 3×10^8 m/s, K is Boltzmann constant with value 8.6173×10^{-5} eV K^{-1}, and T is temperature 293.5 K. Polarizability parameters were calculated to understand the diffusion of the electron cloud in compound. The total dipole moment (μ_{total}), total isotropic polarizability (α_{total}), anisotropy of polarizability ($\Delta\alpha$), and first order hyperpolarizability (β_{total}) can be given as (Rana and Chowdhury 2020; Bhatt et al. 2020; Rana et al. 2020; Huang et al. 2006).

$$\mu_{tot} = (\mu_x^2 + \mu_y^2 + \mu_j^2)^{\frac{1}{2}} \tag{7}$$

$$\alpha_{tot} = \frac{1}{3}(\alpha_{xx} + \alpha_{yy} + \alpha_{zz}) \tag{8}$$

$$\Delta\alpha = \frac{1}{\sqrt{2}}\left[(\alpha_{xx} - \alpha_{yy})^2 + (\alpha_{yy} - \alpha_{zz})^2 + (\alpha_{zz} - \alpha_{xx})^2 + 6\alpha_{xz}^2 + 6\alpha_{xy}^2 + 6\alpha_{yz}^2\right]^{\frac{1}{2}} \tag{9}$$

$$\langle\beta\rangle = \left[(\beta_{xxx} + \beta_{xyy} + \beta_{xzz})^2 + (\beta_{yyy} + \beta_{yzz} + \beta_{zyy})^2 + (\beta_{zzz} + \beta_{zxx} + \beta_{zyy})^2\right]^{\frac{1}{2}} \tag{10}$$

where μ_x, μ_y, and μ_z are the tensor components dipole moment, α_{xx}, α_{yy}, and, α_{zz} are the tensor components of polarizability and β_{xxx}, β_{yyy}, and β_{zzz} are the tensor components of hyperpolarizability.

3 Results and discussion

3.1 Structure

Structures for all the considered AA were optimized to the ground state energy level and were listed in Table 1. Optimized geometry helps in finding the net polarity of the molecule by the means of dipole moment. The more the dipole moment, the more the compound will be polarizable (Lakhera et al. 2021; Visscher and Geerke 2019; Rana et al. 2017). In the present case, the selected EAA **Histidine** (5.58 Debye) has the maximum dipole moment as compared to **Isoleucine** (1.65 Debye), **Leucine** (1.85 Debye), **Lysine** (0.88 Debye), **Methionine** (0.96 Debye), **Phenylalanine** (1.62 Debye), **Threonine** (2.50 Debye), **Tryptophan** (2.95 Debye), and **Valine** (1.31 Debye) (SD 1). The optimal bond lengths are inversely related to the bond strength and the stability of the bond. The lesser the bond length more will be the stability of the bond. Although, the bond angle is inversely proportional to the bond length. Some selected bond lengths and bond angles for the

optimized geometries corresponding to the charge transfer parts of the AA are mentioned in Tables 2 and 3. All the AA possess non-planar geometries. The **Histidine** molecule has dihedral angles C8–C6–C7–C9 and C8–C6–C7–N4. It consists of a carboxyl group and an amino group and its side chain has a basic group containing an imidazole ring. The low values of bond lengths also result in high bond dissociation energy. The 1O–20H bond of the carboxyl group has the lowest bond length of 0.977 Å which showed the stability of the bond. The bond 7C–6C of the alkyl group has the maximum bond length (1.54 Å). Thus, this bond might possess low bond dissociation energy. The angle associated with the pyrrolidine ring 16H–10C–8C has a minimum bond angle of 29.29° which indicated the strength of the pyrrolidine ring. **Isoleucine** has a carboxyl group and amino group connected to a 5C atom. The carbon chain showed the non-planarity of the molecule. The angle between the 1O–9C–2O bond of the carboxyl group is 122.65° and the angle 20H–3N –21H of the amino group is 106.31°. The bond angle between the carboxyl group is comparatively higher than that between the amino group which shows the high probability of the amino bonds getting dissociated.

The structure of **Leucine** is quite similar to **Isoleucine** having amino and carboxyl groups attached to the 6C atom of the carbon chain. The 22H–1O bond of the carboxyl group in **Leucine** has a minimum bond length of 0.97 Å and bond 6C–3N that connects the amino group with the geometry has a maximum bond length of 1.47 Å.

Unlike **Leucine** and **Isoleucine** (which have single amino group), **Lysine** has two amino groups connected to 8C and 9C atoms and carboxyl connected to 10C atoms. The molecule consists of a straight carbon chain without any branched alkanes. However, the bond between the oxygen and hydrogen of the carboxyl group has a minimum bond length of 0.97 Å. The minimal bond lengths showed the strength of these bonds and reflect the charge-accepting behavior of the carboxyl group. The bonds between the nitrogen and hydrogen atoms of amino groups are close for both the amino groups and quite higher than the bond lengths associated with the carboxyl group. The bond angle 1O–10C–2O (122°) associated with the carboxyl group also shows the accepting nature of the carboxyl group.

The amino and carboxyl groups of the **Methionine** molecule are connected to a 6C atom of a carbon chain. Apart from amino and carboxyl groups, one sulphur atom 1S is also connected to the 7C atom of a carbon chain. Being both π- and σ-donor, 1S atom might impart in being the charge donating moiety. The bond length of the 1S–7C bond is 1.90 Å which was the highest of all the bond lengths. The bond lengths corresponding to amino groups like 15H–4N (1.01 Å) and 16H–4N (1.01 Å) are less than the bonds corresponding to the carboxyl group like 8C–2O (1.38 Å).

Phenylalanine has a benzene ring attached to a 4C atom and one amino and carboxyl group were attached to a 5C atom. Dihedral angle 6C – 4C – 5C – 3N is seen to be responsible for the non-planer geometry of **Phenylalanine**. The bond 5C–9C of the carbon chain has a maximum bond length of 1.51 Å. The bonds 18H–3N and 19H–3N have high bond lengths of 1.00 Å and 1.01 Å respectively. These bond lengths are lower than the bond length 23H–1O corresponding to the carboxyl group 0.97 Å. The higher bond length of the amino group reveals the tendency of these bonds of getting easily dissociated.

The amino and carboxyl groups in the **Threonine** are attached to a 6C atom. Apart from these two groups, one hydroxyl group is also attached to the 5C atom. The bond lengths 17H–2O (0.97 Å) and 16H–1O (0.97 Å) associated with the carboxyl group were less in magnitude than the bonds 14H–4N (1.01 Å) and 15H–4N (1.01 Å) associated to the amino group. The bond angle 2O–8C–3O with a magnitude of 122.406° is also greater than bond angles 14H –4N–15H (111.48°) displays the high chances of dissociation of amino bonds.

Table 2 Bond lengths corresponding to functional groups of the optimized structures of EAA (Bond length is in Å)

Bond	Bond length	Bond	Bond length
Histidine			
1O – 9C	1.37	4 N – 17H	1.01
2O = 9C	1.23	4 N – 18H	1.01
20H – 1O	0.97	3 N – 11C	1.37
C8 = C10	1.37	5 N – 11C	1.33
Isoleucine			
22H – 1O	0.98	20H – 3 N	1.01
1O – 9C	1.35	21H – 3 N	1.01
9C = 2O	1.22	5C – 3 N	1.46
Leucine			
22H – 1O	0.97	20H – 3 N	1.00
1O – 9C	1.37	21H – 3 N	1.01
9C = 2O	1.23	6C – 3 N	1.47
Lysine			
1O – 24H	0.97	20H – 3 N	1.01
1O – 10C	1.38	21H – 3 N	1.01
10C = 2O	1.23	22H – 4 N	1.01
10C – 8C	1.52	23H – 4 N	1.01
Methionine			
3O = 8C	1.23	15H – 4 N	1.01
8C – 2O	1.38	16H – 4 N	1.01
2O – 20H	0.97	1S – 7C	1.90
Phenylalanine			
23H – 1O	0.97	18H – 3 N	1.00
1O – 9C	1.37	19H – 3 N	1.01
9C = 2O	1.23	5C – 9C	1.51
Threonine			
17H – 2O	0.97	14H – 4 N	1.01
2O -8C	1.38	15H – 4 N	1.01
8C = 3O	1.23	4 N – 6C	1.45
16H – 1O	0.97	8C – 6C	1.51
Tryptophan			
1O – 27H	0.97	24H – 4 N	1.01
1O – 13C	1.37	25H – 4 N	1.01
13C = 2O	1.23	3 N – 20H	1.00
10C – 3 N	1.39	9C – 3 N	1.38
Valine			
1O – 19H	0.97	17H – 3 N	1.01
8C = 2O	1.23	18H – 3 N	1.01

Tryptophan consists of a benzene ring and a pyrrolidine ring mutually connected with 7C–9C bond. The bonds 24H–4N (1.01 Å) and 25H–4N (1.01 Å) of the amino group have higher bond lengths than the bond 1O–27H (0.97 Å).

Valine molecule comprises one amino and one carboxyl group attached to a 5C atom. The 1O–19H bond of the carboxyl group has a bond length of 0.97 Å which is less than the

Table 3 Bond angles corresponding to functional groups of the optimized structures of EAA (Bond angle is in °)

Bond	Bond angle	Bond	Bond angle
Histidine			
20H – 1O – 9C	111.07	8C – 3 N – 15H	123.62
1O – 9C – 2O	121.32	15H – 3 N – 11C	128.47
2O – 9C – 7C	127.31	11C – 5 N – 10C	105.46
Isoleucine			
22H– 1O – 9C	111.87	21H – 3 N – 20H	106.31
1O – 9C – 2O	122.65	3 N – 5C – 9C	105.61
Leucine			
22H– 1O – 9C	110.37	21H – 3 N – 20H	113.01
1O – 9C – 2O	122.07	3 N – 6C – 9C	104.87
Lysine			
22H – 4 N – 23H	111.32	24H – 1O – 10C	110.69
20H – 3 N – 21H	110.66	1O – 10C – 2O	122.00
Methionine			
20H – 2O – 8C	110.65	15H – 4 N – 16H	110.37
2O – 8C – 3O	121.64	7C – 1S – 9C	99.56
Phenylalanine			
23H – 10 – 9C	110.59	18H – 3 N – 19H	113.56
1O – 9C – 2O	122.44	18H – 3 N – 5C	115.26
Threonine			
17H – 2O – 8C	110.92	14H – 4 N – 15H	111.48
2O – 8C – 3O	122.40	16H – 1O – 5C	111.14
Tryptophan			
27H – 1O – 13C	110.74	24H – 4 N – 25H	111.22
1O – 13C – 2O	122.22	9C – 3 N – 20H	125.58
9C – 3 N – 10C	109.16	10C – 3 N – 20H	125.24
Valine			
19H – 1O – 8C	110.49	17H – 3 N – 18H	110.74
1O – 8C – 2O	121.62	2O – 8C – 5C	125.49

bond length of 17H–3N (1.01 Å). The increasing order of electrostatic potential energies of the AA was **Methionine < Tryptophan < Phenylalanine < Histidine < Lysine < Leucine < Isoleucine < Threonine < Valine** (SD 1). Negative magnitudes of electrostatic potential reflect the tendency of the molecule to attract the charge density. The optimized structures of all the AA indicated that the bond lengths and bond angles corresponding to the amino groups are smaller than the bond lengths and bond angles corresponding to carboxyl groups which shows the enhanced chances of dissociations of amino bonds. This in turn, shows the possibility of intramolecular interactions within the molecules that reveals the reactivity of the AA.

3.2 Charge analysis

Mulliken charge analysis helps in the understanding of the charge contribution corresponding to each atom of the systems (Senthilkumar et al. 2021). The charge plot of

EAA shows the positive charge impact of H atoms and the negative charge contribution of O atoms (Fig. 1). The charges corresponding to each atom of the **Histidine** molecule are plotted in Fig. 1(a). 9C and 20H atoms of the carboxyl group of **Histidine** showed the maximum positive charge of 0.54 e and 0.39 e respectively. The 3N and 5N atoms associated with the pyrrolidine ring show a negative charge of − 0.73 e and − 0.37 e respectively. The 4N, 17H and 18H atoms of the amino group have charges of − 0.67 e, 0.30 e, and 0.29 e respectively. The Mulliken charge distribution of **Histidine** showed the huge variation in charge between the pyrrolidine ring and carboxyl and amino groups. The Mulliken charge plot of **Isoleucine** is shown in Fig. 1(b). In **Isoleucine**, the charge variation is observed among the 1O (-0.55 e), 2O (-0.36 e), 9C (0.47 e) and 22H (0.38 e) atoms of carboxyl group and 3N (-0.64 e), 20H (0.29 e) and 21H (0.38 e) of amino group. Similar kind of variation of charge is observed in **Leucine** molecule in 1O (-0.55 e), 2O (-0.38 e), 9C (0.55 e) and 22H (0.38 e) atoms of carboxyl group and 3N (-0.69 e), 20H (0.29 e) and 21H (0.3 e) of amino group. Two amino groups in **Lysine** with atoms 3N (− 0.66 e), 20H (0.29 e), 21H (0.29 e), and 4N (− 0.71 e), 22H (0.28 e), 23H (0.28 e) and a carboxyl group with atoms 1O (− 0.56 e), 2O (− 0.36 e), 10C (0.45 e) and 24H (0.38 e) showed the immense charge variation. The Mulliken charge distribution of the atoms in **Methionine** is illustrated in Fig. 1(e). Charge distribution predicts that the 8C atom of the carboxyl group shows the highest magnitude of positive charge equal to 0.48 e and the 4N atom of the amino group shows the negative charge of − 0.72 e. Thus, these atoms reflect the major charge variation in the **Methionine** molecule. In **Phenylalanine**, the 9C atom of the amino group has the maximum positive charge and the 3N atom of the carboxyl group have a negative charge with a maximum magnitude of -0.69 e. Mulliken charge distribution of the rest of the atoms of **Phenylalanine** is shown in Fig. 1(f). The **Threonine** molecule has an –OH (hydroxyl) group connected to the C5 atom of the carbon chain with atoms 1O and 16H with a charge of -0.60 e and 0.36 e respectively (Fig. 1(g)). Apart from this, the 8C atom of the carboxyl group has a maximum positive charge of 0.53 e. The 4N atom of the amino group of **Threonine** has a charge of -0.68 e. Thus, the charge variations is among the atoms of hydroxyl, carboxyl, and amino groups. The 3N atom connected to the pyrrolidine ring in the **Tryptophan** molecule has the highest magnitude of negative charge -0.81 e. The 3C atom of the carboxyl group has the highest positive charge 0.53 e (Fig. 1(h)). These atoms impart the major charge variation in **Tryptophan**. In **Valine**, the 8C atom of the carboxyl group shows the highest charge of 0.50 e, and the 3 N atom of the amino group has a charge of -0.68 e. The rest of the Mulliken charge distribution for **Valine** is illustrated in Fig. 1(i). The variation in charge is observed between the functional groups (say amino and carboxyl groups). This variation can be considered due to the delocalization of the charges from the carboxyl part to the amino part of the molecule. This may lead to enhanced intramolecular interactions within the molecule. Therefore, the AA can be considered chemically reactive.

3.3 Chemical reactivity

FMO theory is a practical model which describes the chemical reactivity of the molecule (Swartling et al. 2018). The energy corresponding to HOMO and LUMO are termed as FMO energies (Saito et al. 2020). HOMO is the electron donating orbital and LUMO is the electron accepting orbital (Rana et al. 2016). The HOMO–LUMO map of different probe systems is shown in Fig. 2, which represents the distribution of highest

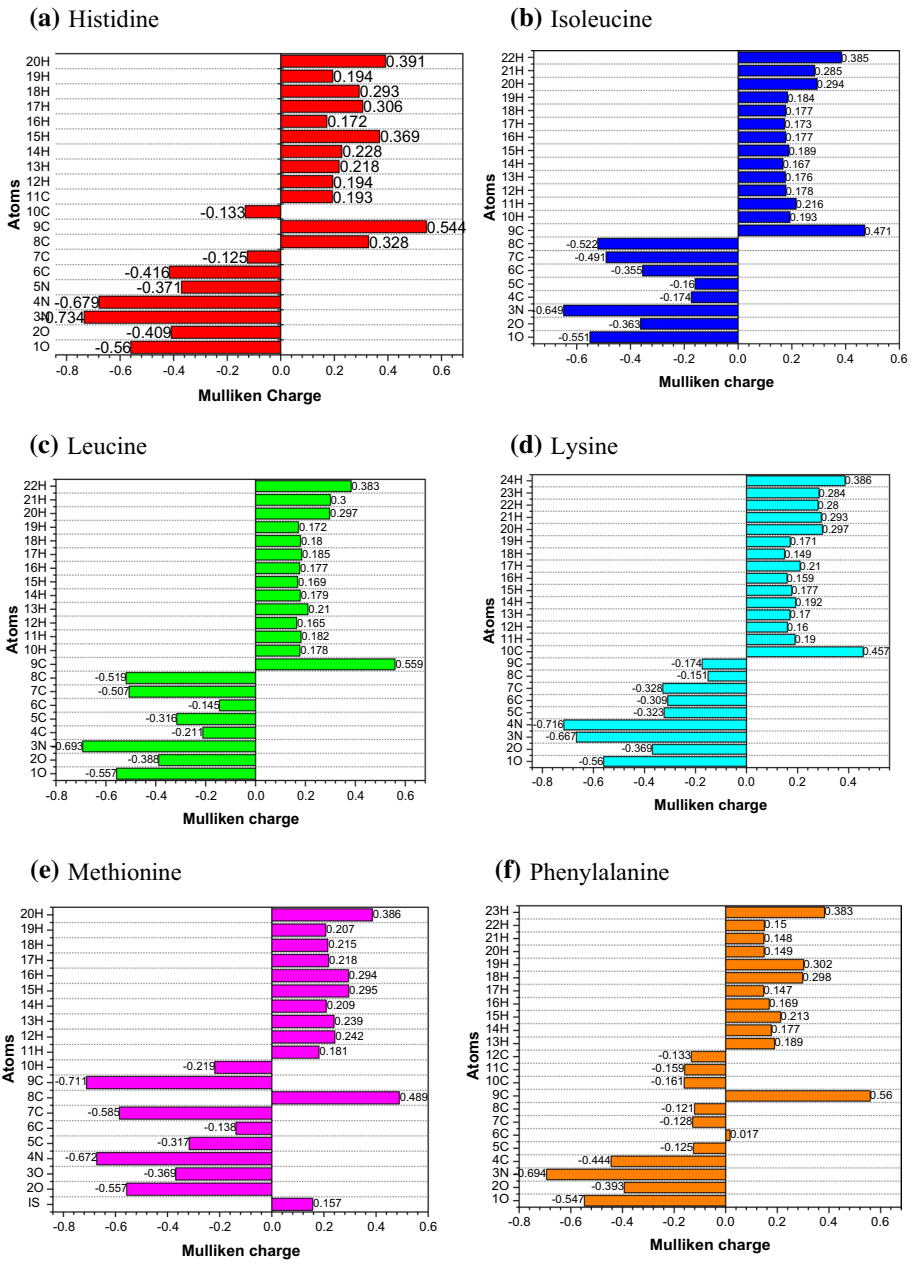

Fig. 1 Mulliken charge plot for EAA showing positive charge impact of hydrogen atoms and negative impact of nitrogen and oxygen atoms

occupied orbitals throughout the geometry and the distribution of lowest occupied orbitals in the functional groups. There is significant energy associated with these orbitals.

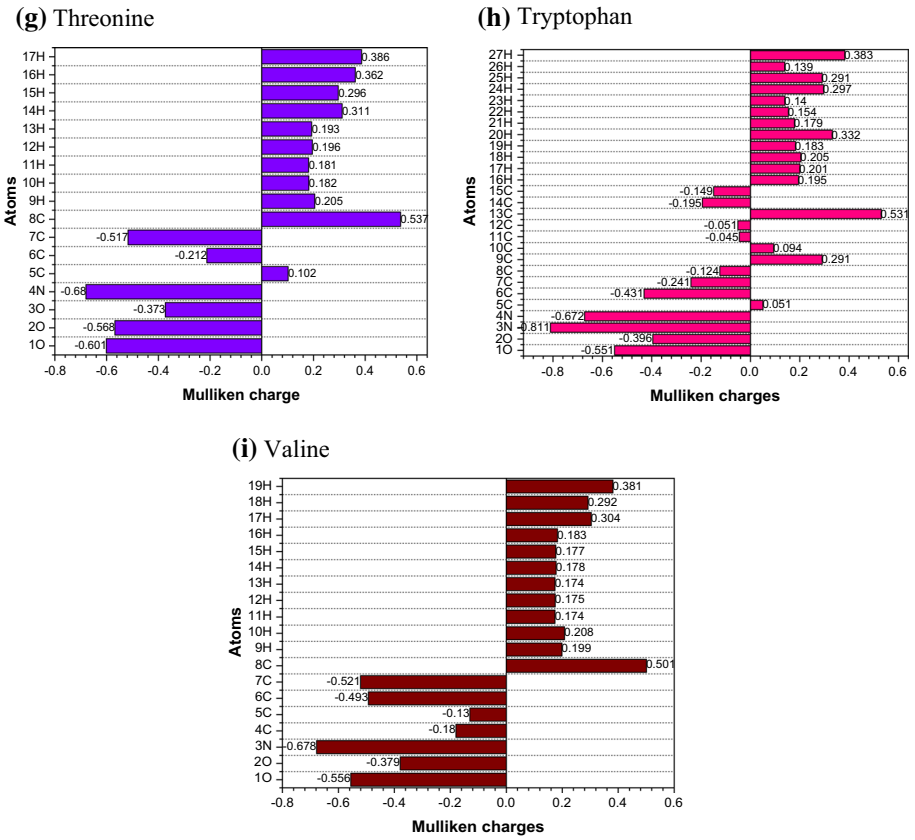

Fig. 1 (continued)

The computed values of FMO parameters of all the AA are mentioned in Table 4. The energy difference between the LUMO and HOMO energies is called band gap (ΔE). The low value of ΔE validates the easy excitation tendency of the free electron cloud from the lower states to the higher energy states. The value of ΔE for **Histidine** is 4.97 eV. This value is lower than **Isoleucine** (5.99 eV), **Leucine** (5.95 eV), **Lysine** (5.42 eV), **Methionine** (5.60 eV), **Phenylalanine** (5.82 eV), **Threonine** (6.02 eV), **Tryptophan** (5.11 eV), and **Valine** (5.93 eV). The values of ΔE for all the **AA** are found to be lower than the ΔE values of reference materials like Urea (7.43 eV) and KDP (6.83 eV). The low value of the energy gap shows the high possibility of the charge transfer within the molecule. The increasing order of ΔE values for AA is **Histidine < Tryptophan < Lysine < Methionine < Phenylalanine < Valine < Leucine < Isoleucine < Threonine**. The *IP* shows the potential that is needed to eject the electron from the nucleophilic atom. The values of *IP* for **Histidine**, **Isoleucine**, **Leucine**, **Methionine**, **Phenylalanine**, **Threonine**, and **Valine** are 6.20, 6.47, 6.39, 6.23, 6.34, 6.73, and 6.52 eV. These values are higher than *IP* for **Lysine** (5.94 eV) and **Tryptophan** (5.61 eV). The increasing order of *IP* was **Tryptophan < Lysine < Histidine < Methionine < Phenylalanine < Leucine < Isoleucine < Valine < Threonine**. This showed that **Tryptophan** has a better capability to donate

the charge easily than the other AA. The *EA* is a measure of the magnitude of energy that is liberated while attracting the free-charge cloud. The high values of *EA* show that the molecule accepts the free charge cloud more easily. **Histidine** has the highest value of *EA* equal to 1.22 eV. The values of *EA* for other AA are **Isoleucine** (0.48 eV), **Leucine** (0.43 eV), **Lysine** (0.51 eV), **Methionine** (0.62 eV), **Phenylalanine** (0.52 eV), **Threonine** (0.70 eV), **Tryptophan** (0.50 eV), and **Valine** (0.59 eV). The increasing order of *IP* is **Leucine < Isoleucine < Tryptophan < Lysine < Phenylalanine < Valine < Methionine < Threonine < Histidine**. So, the **Histidine** molecule has the maximum value of *EA* showing its enhanced capability of attracting the charge cloud. The values of *CP* in raising order are **Threonine** (-3.16 eV) < **Histidine** (− 3.71 eV) < **Valine** (− 3.55 eV) < **Isoleucine** (− 3.48 eV) < **Phenylalanine** (− 3.43 eV) < **Methionine** (− 3.42 eV) < **Leucine** (− 3.41 eV) < **Lysine** (− 3.22 eV) < **Tryptophan** (− 3.05 eV). As the lower *CP* is considered the most stable one, the **Threonine** can be considered as the molecule undergoing the chemical process more easily with associating low amount of energy. The higher the value of χ, the more strongly the electrophilic it will be able to pull the free charges towards itself. **Threonine** has the highest value of χ which shows that it can strongly attract the shared electrons. The χ is minimum for **Tryptophan** (3.05 eV) and the value raised in order: **Tryptophan < Lysine < Leucine < Methionine < Phenylalanine < Isoleucine < Valine < Histidine < Threonine**. The η gives the extent of the chemical hardness of the molecule or it accounts for the resistance of the molecule towards deformity after undergoing a chemical reaction. The molecules with higher values of η can be considered more chemically stable. **Threonine** has the highest η equal to 3.01 eV as compared to the other AA. On contrary, the *S* is the opposite of η and was used to show the reactivity of the molecules (Akinyele et. al 2022). The molecules with high values of softness are easily deformed or get dissociated while involved in the chemical reaction. Thus, low values of *S* are considered good for a chemically reactive molecule. The *S* is in order: **Isoleucine = Threonine < Leucine < Valine < Phenylalanine < Methionine < Lysine < Tryptophan < Histidine**. It is observed that **Isoleucine** and **Leucine** have the equally lowest values of *S* showing their chemical stability to other AA by the virtue of *S*. However, the difference between the magnitudes of FMO parameters of other AA is not much observable. Thus, it can be said that the AA are chemically reactive and they can be involved in chemical reactions.

The settlement of the HOMO–LUMO surfaces for AA is illustrated in Fig. 2. These surfaces show the location of the orbitals in the molecular orbital wave function, respectively. The HOMO shows the donor orbitals (positive) and LUMO shows the acceptor orbitals (negative). The HOMO–LUMO surfaces of the **Histidine** molecule (Fig. 2(a)) are seen to get drifted from the pyrrolidine ring toward the amino and carboxyl group. A similar kind of surface dislocation is seen in **Lysine** (Fig. 2(d)), **Methionine** (Fig. 2(e)), and **Tryptophan** (Fig. 2(h)). In **Lysine**, the positive and negative surfaces are settled over the amino group in HOMO and get drifted over the carboxyl group in LUMO. This shows the displacement of the charge cloud from amino to the carboxyl group in **Lysine**. **Methionine** has positive and negative surfaces settled over S1 atom in HOMO while they are settled over functional groups in LUMO. In **Tryptophan**, the positive and negative surfaces shift from benzene ring and pyrrolidine ring towards amino and carboxyl group. The shifting of the surfaces shows the direction of the shifting of the charge cloud. The shifting of orbitals in the rest of the AA was not that far as in the former described AA. The orbitals in **Isoleucine** (Fig. 2(b)), **Leucine** (Fig. 2(c)), **Phenylalanine** (Fig. 2(f)), **Threonine** (Fig. 2(g)) and **Valine** (Fig. 2(i)) are uniformly distributed over the geometries and are locally shifted. The orbitals in **Isoleucine** and **Leucine** seemed to shift among the

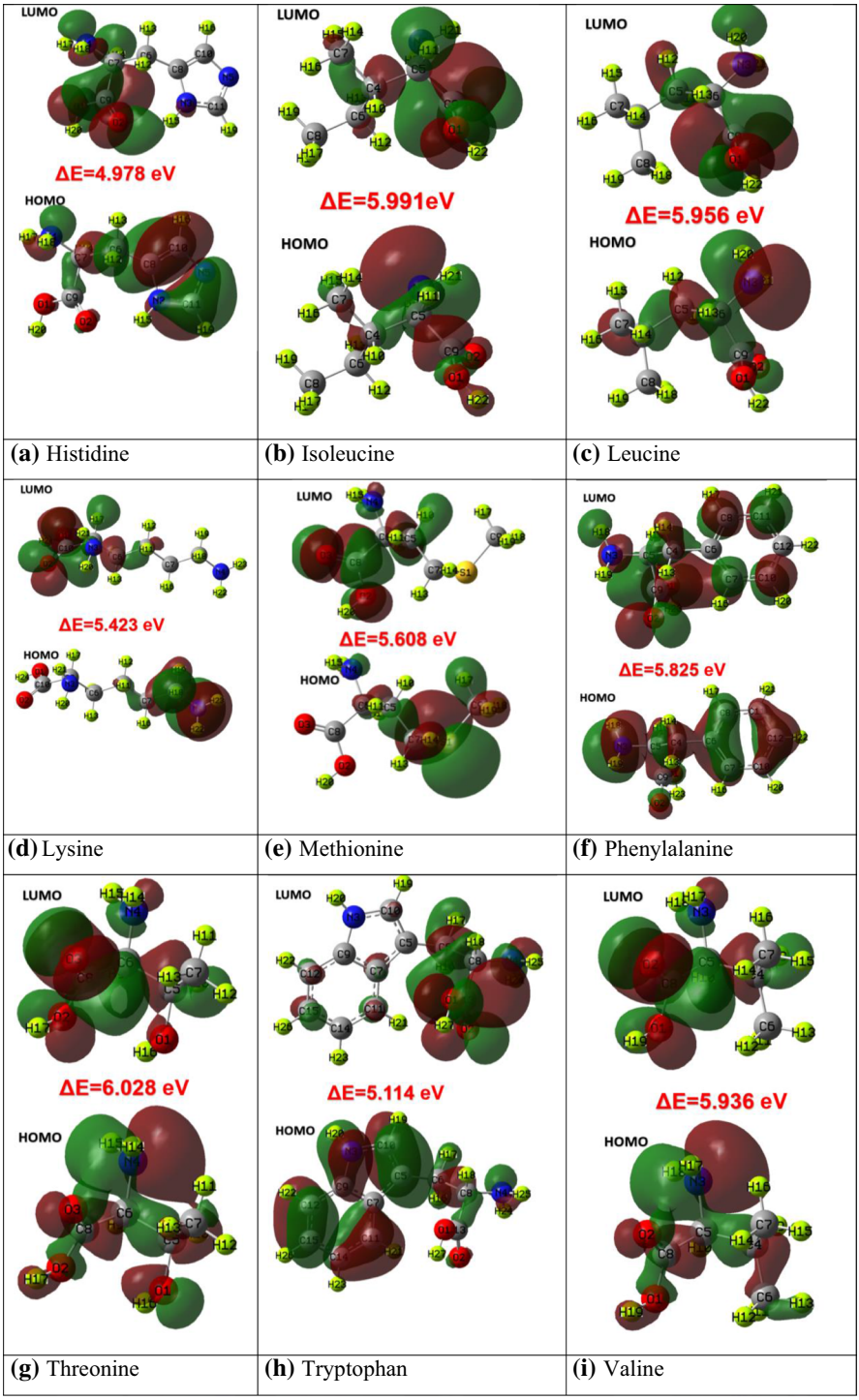

Fig. 2 HOMO–LUMO map for AA

Table 4 Values of global reactivity parameters for AA (all values are in eV and S is in $(eV)^{-1}$)

Molecular property	Histidine	Isoleucine	Leucine	Lysine	Methionine	Phenylalanine	Threonine	Tryptophan	Valine
HOMO	− 6.20	− 6.47	− 6.39	− 5.94	− 6.23	− 6.34	− 6.73	− 5.61	− 6.52
LUMO	− 1.22	− 0.48	− 0.43	− 0.51	− 0.62	− 0.52	− 0.70	− 0.50	− 0.59
Energy gap (ΔE)	4.97	5.99	5.95	5.42	5.60	5.82	6.02	5.11	5.93
Ionization potential (IP)	6.20	6.47	6.39	5.94	6.23	6.34	6.73	5.61	6.52
Electron affinity (EA)	1.22	0.48	0.43	0.51	0.62	0.52	0.70	0.50	0.59
Chemical potential (CP)	− 3.71	− 3.48	− 3.41	− 3.22	− 3.42	− 3.43	− 3.71	− 3.05	− 3.55
Electronegativity (χ)	3.71	3.48	3.41	3.22	3.42	3.43	3.71	3.05	3.55
Hardness (η)	2.48	2.99	2.97	2.71	2.80	2.91	3.01	2.55	2.96
Softness (S)	0.40	0.33	0.33	0.36	0.35	0.34	0.33	0.39	0.33

functional groups. That means red colored surface seems to be replaced by green and vice versa. This shows that the charge transfer occurred between the atoms of the respective amino and carboxyl groups of **Isoleucine** and **Leucine**. In **Phenylalanine**, a red color surface appeared over the amino and carboxyl group in the HOMO surface that transited to the red surface in the LUMO surface. A similar kind of shifting of positive and negative orbitals is observed in **Threonine** and **Valine**. Thus, it is observed that the presence of functional groups induces the shifting of donor and acceptor surfaces in AA. This shifting can be considered due to the dislocation of the charge cloud. Thus, the dislocation of the charge cloud gives rise to immense ICT within the title molecule. Moreover, it can be said that the FMO parameters and HOMO–LUMO surfaces showed the enhanced possibility of ICT within the AA and making them chemically reactive molecules.

3.4 Molecular electrostatic potential (MEP) analysis

The displacement of the charge cloud is provided by the MEP surface color code. The red and yellow color of the MEP is due to the electrophilic atoms (Sheikhi et al. 2019). Mainly the nitrogen atoms are electron donating and the oxygen atoms are electron-withdrawing (Lakhera et al. 2022a, b, c, d,). The O atoms being highly electronegative imparts the red color of the MEP surface (Pathade and Jagdale 2020). The MEP surface of all the AA is illustrated in Fig. 3. This surface indicates the availability and location of the nucleophilic and electrophilic regions of the AA (Lakhera et al. 2022a, b, c, d,). This surface shows the displacement of the charge cloud from the positive part toward the negative part of the AA.

For the **Histidine** molecule, the variation of the charge is seen among the 1O, 2O, 9C, and 20H atoms of the carboxyl group and 4N, 17H, and 18H atoms of the amino group. Being highly resonating, the amino group and carboxyl group imparts in donating the free electron cloud. The pyrrolidine ring, on the other hand, acts as an electron-withdrawing group. Thus, these groups give rise to the nucleophilic and electrophilic regions in the MEP. Thus, the ICT is seen from the amino group and carboxyl group towards the pyrrolidine ring. The MEP's counterplots were also used for the representation of the regions having an electrostatic field of AA. The area with dense counter lines is the area with a stronger electrostatic field (Idouhli et al. 2021). The field lines are found denser near the 2O atom of the carboxyl group and the 5N atom of the pyrrolidine ring. The regions near 4N, 5N, and 2O atoms have a high electrostatic field (Fig. 4(a)). The bonds falling in the region of the aligned electrostatic field undergo the simultaneous shortening and elongation of the bond. Therefore, this process leads to the weakening of the bonds, and ultimately breaking the bond. Thus, the bonds surrounded by dense electrostatic field counter lines are weak enough to get dissociate. This leads to the formation and displacement of free electron cloud which is a key of ICT. The **Histidine** molecule, therefore, has the field lines largely accumulated near the carboxyl group, amino group, and pyrrolidine ring that validates the ICT between the functional groups as stated from Mulliken charge distribution and MEP surface.

In the MEP surface of AA like **Isoleucine** (Fig. 3(b)), **Leucine** (Fig. 3(c)), **Lysine** (Fig. 3(d)), **Methionine** (Fig. 3(e)), **Phenylalanine** (Fig. 3(f)), **Threonine** (Fig. 3(g)), and **Valine** (Fig. 3(i)), it was seen that the C=O bond of the carboxyl contributes in formation of red surface while the O – H bond imparts the blue color to the MEP surface. The ICT in these molecules was seen to get dislocated from the amino group towards the carboxyl group. The counterplots of the **Isoleucine** (Fig. 4(b)), **Leucine** (Fig. 4(c)), **Lysine** (Fig. 4(d)), **Methionine** (Fig. 4(e)), **Phenylalanine** (Fig. 4(f)), **Threonine** (Fig. 4(g)),

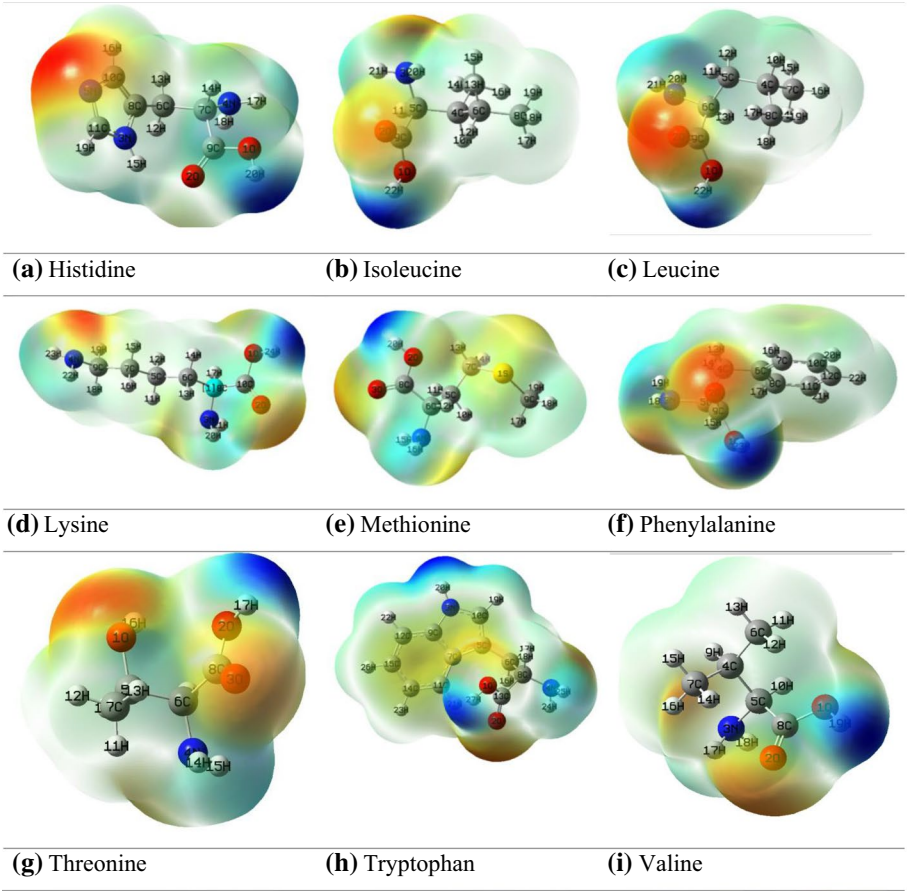

Fig. 3 Molecular electrostatic potential surface of essential amino acids illustrating electrophilic region in blue and nucleophilic region in red colour

and **Valine** (Fig. 4(i)) are highly accumulated near the functional groups in the respective molecules. This validates the ICT predicted by the MEP surface. The bonds of the functional groups have electrostatic field counter lines nearby that will lead to the weakening and dissociation of the bonds. This, in turn, can be considered the main reason for the evolution of the charge cloud from these functional groups and inducing ICT within the AA. The MEP surface of **Tryptophan** AA is illustrated in Fig. 3(h)). Similar to **Histidine**, **Tryptophan** also has a pyrrolidine ring that acted as a nucleophilic part. The yellow color is uniformly spread over the benzene ring connected to the pyrrolidine ring showing the negativity of the benzene ring. The 4N, 24H, and 25H of the phenol group, and 1O, 2O, 13C, and 27H atoms of the carboxyl group, however, impart the blue color indicating the donation of charge cloud from these regions. Thus, the ICT in **Tryptophan** is seen from the pyrrolidine ring, carboxyl, and amino group towards the benzene ring. The counterplot of **Tryptophan** is illustrated in Fig. 4(h). Alike the other AA, the counterplot lines in **Tryptophan** are finely spread over the carboxyl and amino groups showing the evolution of the charge cloud from these regions. Thus, the presence of nucleophilic and

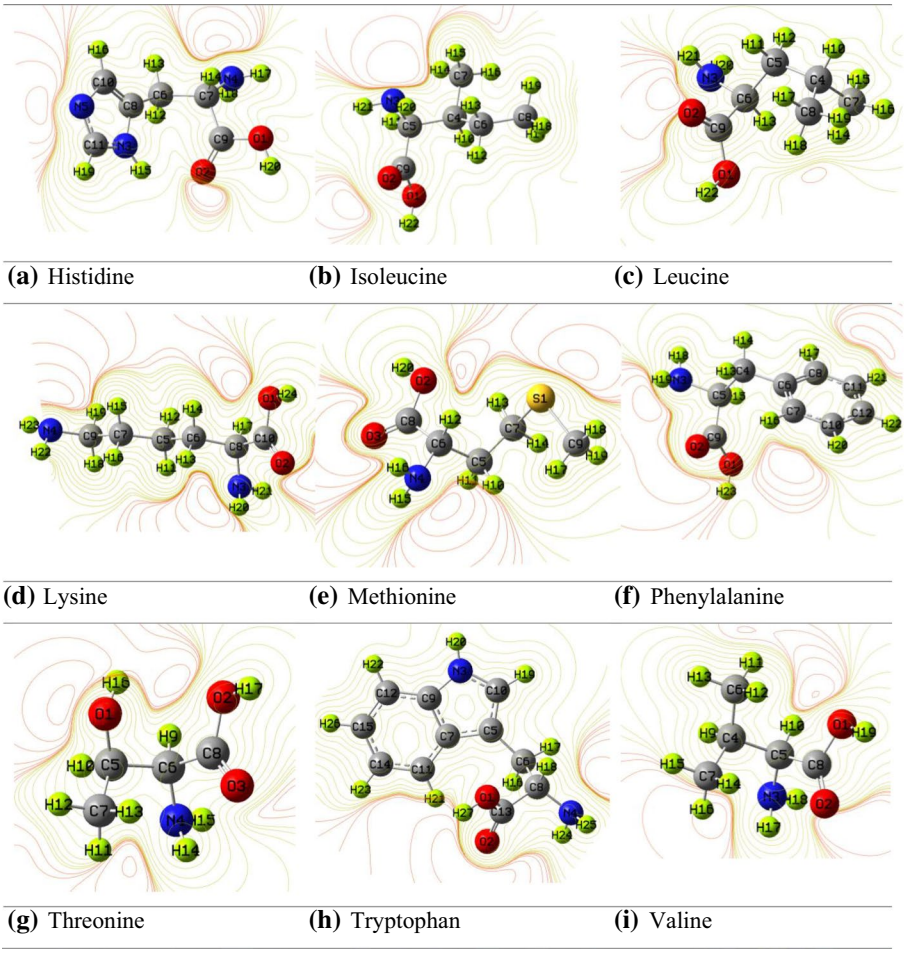

(a) Histidine **(b)** Isoleucine **(c)** Leucine

(d) Lysine **(e)** Methionine **(f)** Phenylalanine

(g) Threonine **(h)** Tryptophan **(i)** Valine

Fig. 4 Counter plots showing high electrostatic field of the AA

electrophilic regions validates the high degree of electrostatic interactions within the molecule. This show that there is a possibility of charge transfer from the nucleophilic region to the electrophilic region. Thus, the variation of the electronic distributions within the molecule gives a possibility of the molecule being a highly reactive molecule.

3.5 Vibrational analysis

The Raman modes are investigated for AA to study its vibrational features. The Raman spectra help in studying the polarizing ability of the compound as the polarizability of any compound is proportional to the Raman intensity, which in turn leads to the NLO behavior of the compound (John et al. 2020; Prettre and Pullman 1987). The computed Raman spectra for all the AA are shown in Fig. 5. High-frequency vibrations are observed for AA

in the range of 1000–2000 cm^{-1} and 2500–4000 cm^{-1}. The vibrational modes with high peaks with their corresponding Raman intensities are mentioned in SD 2.

For the **Histidine** molecule, the symmetric stretching (ν_{OH}) mode is observed at 3637.7 cm^{-1}. The 17H – 4N – 18H atoms of the amino group show ν_{NH} mode at 3516.02 cm^{-1}. The ν_{CH} modes of the **Histidine** showed three major peaks at 3012.7 (ν_{6C-12H} and ν_{6C-13H}), 3098.73 (ν_{6C-12H} and ν_{6C-13H}), and 3271.1 cm^{-1} ($\nu_{10C-16H}$ and $\nu_{11C-19H}$). The 8C=10C bond of the benzene ring shows ν_{CC} mode at frequency 1602.72 cm^{-1}. The torsional bending of the C – H bond on the plane (δ_{CH}) mode shows the bending of the bond between 6C – 12H and 7C – 14H bonds in the plane. However, these modes corresponding to the carbon chain have the maximum Raman intensity equal to 1631.56 cm^{-1}. Figure 5(a) illustrated the computed Raman spectra of **Histidine**.

For **Isoleucine**, the ν_{OH} mode is observed at 3583.26 cm^{-1}. The 17H – 4N – 18H atoms of the amino group show ν_{NH} and asymmetric linear stretching (α_{NH}) mode at 3436.4 and 3515.96 cm^{-1} respectively. The ν_{CH} mode of the **Isoleucine** has a major peak at 2992.93 cm^{-1} leading to the stretching of the hydrogens bonded with 6C, 7C, and 8C atoms of the carbon chain. The asymmetric stretching of C – H bonds have two major peaks, one at 3023.95 cm^{-1} (α_{5C-11H}) and another at 3055.33 cm^{-1} (C–H bonds attached to 7C and 8C). The δ_{CH} modes show the bending of the bond between 1143.7 to 1528.86 cm^{-1}. The stretching between 4C – 6C atoms of carbon chain shows mode at 793 cm^{-1}. Figure 5(b) illustrated the computed Raman spectra of **Isoleucine**.

The **Leucine** molecule has α_{NH} mode of 3N – 20H and 3N – 21H at frequency 3641.67 cm^{-1}. The stretching between 1O – 22H of the carboxyl group is observed at 3623.64 cm^{-1}. ν_{NH} mode of amino group bonds 3N – 20H and 3N – 21H is observed at frequency 3641.67 cm^{-1}. Three sharp peaks are observed for stretching of C – H bonds at 2978.01, 3016.4, and 3081.21 cm^{-1}. Twenty modes of bending of C – H bonds were observed in the range 975.95–1529.85 cm^{-1}. High Raman intensity of 1637.03 cm^{-1} is observed for the C – C bond of the carbon chain for mode 782.41 cm^{-1}. The computed Raman spectra of **Leucine** are illustrated in Fig. 5(c).

The Raman spectra of **Lysine** (Fig. 5(d)) have three high-intensity peaks at 2906.07, 2984.77, and 3051.01 cm^{-1} showing ν_{CH} modes of the 8C – 6C – 5C – 7C – 9C chain. The 10C=2O bond of the carboxyl chain showed ν_{CO} mode at 1711.01 cm^{-1}. The δ_{CH} mode shows the bending modes from 1000.04 to 1528.41 cm^{-1}.

The 2O – 20H bond of the carboxyl group of **Methionine** vibrates linearly at 3623.06 cm^{-1}. The 16H – 4N – 15H bond of the amino group in **Methionine** shows ν_{NH} vibrational mode at 3499.93 cm^{-1}. There are two high-intensity peaks observed for C – H linear stretching. The vibration of 17H, 18H 19H attached to 9C bound to 1S atom have ν_{CH} mode at 3048.77 cm^{-1}. The α_{CH} for 13H and 14H attached to the 7C atom was observed at 3145.22 cm^{-1}. The ν_{CO} mode between 8C=3O of the carboxyl group is at a frequency of 1709.03 cm^{-1}. The δ_{CH} modes are observed between 1214.06 to 1495.78 cm^{-1}. The vibration of 1S bonded between 7C and 9C has high intensity of 4042.93 cm^{-1} at a frequency of 655.69 cm^{-1}. The ν_{CH} at 588.04 cm^{-1} has the highest Raman intensity of 9103.99 cm^{-1}. The other modes are illustrated in Fig. 5(e).

The computed Raman spectra of **Phenylalanine** are shown in Fig. 5(f). The spectra highlighted the high-frequency mode α_{NH} of the amino group at 3654.76 cm^{-1} and ν_{NH} mode at 3529.77 cm^{-1}. The 1O – 23H atoms of the carboxyl group showed ν_{OH} mode at 3654.03 cm^{-1}. The ν_{CH} vibrations gave sharp peaks between frequency 3023.73 cm^{-1} and 3194.86 cm^{-1}. The δ_{CH} modes were observed between 1030.89 cm^{-1} and 1520.44 cm^{-1}. The ν_{CC} mode between 5C and 9C has a vibration at 762.06 cm^{-1} and the δ_{CC} mode of the benzene ring occurs at 653.65 cm^{-1}.

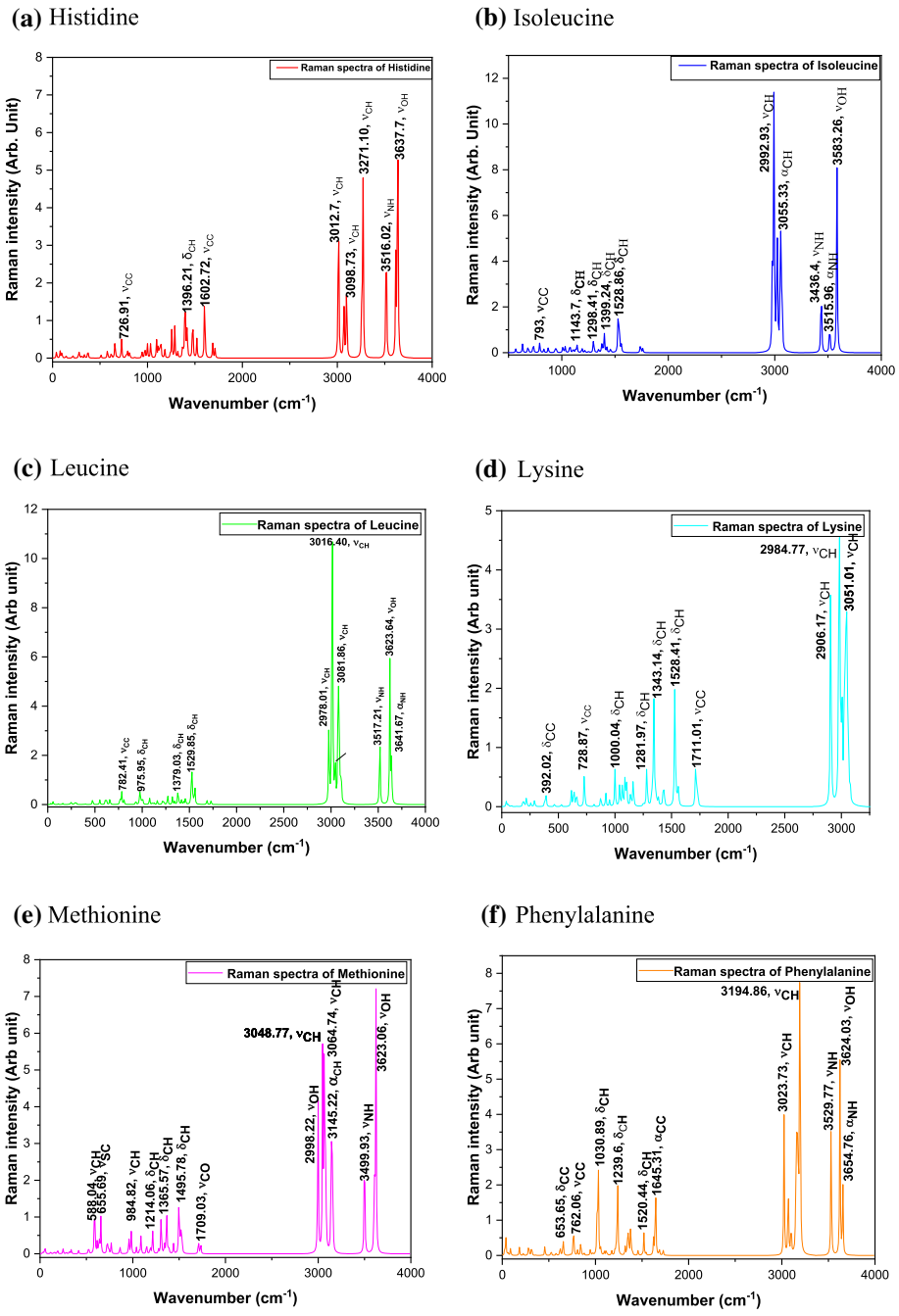

Fig. 5 Computational Raman spectra of EAA showing different modes with maximum frequency (ν- symmetric stretching, α- asymmetric stretching, δ- torsional bending of the mode)

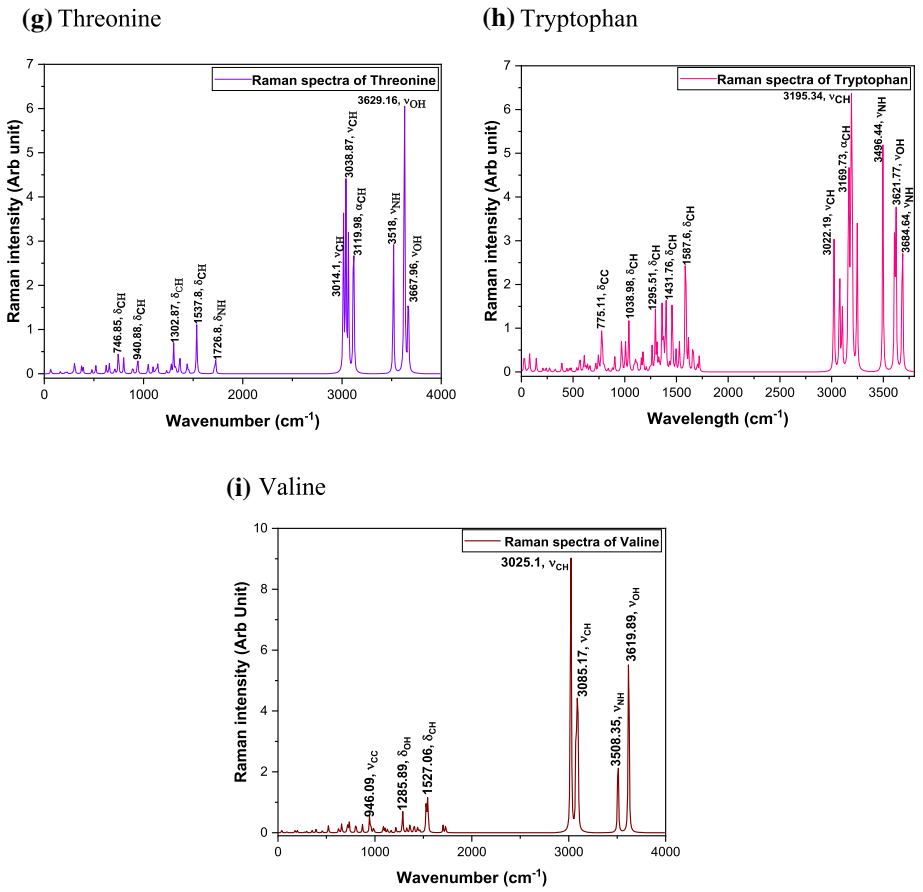

Fig. 5 (continued)

The computed Raman spectra of **Threonine** was shown in Fig. 5(g). There are two high-frequency peaks for ν_{OH} modes of O – H bonds. The ν_{OH} mode for the 1O – 16H bond of the hydroxyl group exists for frequency 3667.96 cm^{-1}. The 4N, 14H and 15H atoms of the amino group have a frequency equal to 3518 cm^{-1} for ν_{NH} and 1726.8 cm^{-1} for δ_{NH} mode. The 2O – 17H bond of the carboxyl group has ν_{OH} mode at 3629.16 cm^{-1}. The 7C atom of the carbon chain has two different modes, first ν_{CH} at 3038.87 cm^{-1} and second α_{CH} at 3119.98 cm^{-1}. The δ_{CH} modes are observed between 746.85 and 1537.8 cm^{-1}. However, the δ_{CH} mode at frequency 746.85 cm^{-1} has the highest intensity of 2012.59 cm^{-1}.

The **Tryptophan** has one pyrrolidine ring attached to the carbon chain and a benzene ring. The 3N – 20H bond of the pyrrolidine ring has ν_{NH} mode at 3684.64 cm^{-1}. The ν_{NH} mode corresponding to amino bonds 4 N – 25H and 4 N – 25H has a frequency of 3496.44 cm^{-1}. The 1O – 27H bond of the carboxyl group has mode ν_{CH} at 3621.77 cm^{-1}. The α_{CH} mode is for the stretching of C – H bonds of benzene rings (11C – 21H, 12C – 22H, and 14C – 23H). The 11C, 12C, 14C, and 15C atoms of the benzene ring vibrate simultaneously and lead to the highest intensity mode for C – H bonds with a frequency of 3195.34 cm^{-1}. The δ_{CH} modes have multiple peaks between 775.11 to 1659.72 cm^{-1}. However, the δ_{CH} mode at 1587.6 cm^{-1}

is reported as the highest Raman intensity mode with a magnitude of 2423.57 cm^{-1}. The computed spectra of **Tryptophan** are illustrated in Fig. 5(h).

The computed Raman modes of **Valine** are shown in Fig. 5(i). The 1O – 19H bond of the carboxyl group has stretching mode ν_{OH} at 3619.89 cm^{-1}. The ν_{NH} mode between amino group 3N – 17H and 3N – 18H bond exists for frequency 3508.35 cm^{-1}. ν_{CH} modes have two sharp peaks for C – H vibrations of the carbon chain at frequencies 3025.1 cm^{-1} and 3085.17 cm^{-1}. For δ_{CH}, the highest frequency mode is at 1527.06 cm^{-1}. The 1O – 19H bond of the carboxyl group has a frequency of 1285.89 cm^{-1}. The stretching between 4C – 5C is observed at 946.09 cm^{-1}. The highest Raman intensity of 1193.34 cm^{-1} is observed for ν_{CC}. The spectral analysis done for the AA showed the high Raman intensity for the modes associated with the functional groups present in the AA showed the high chemical reactivity of these groups. All the above-mentioned Raman modes reveal the strong activity of the AA. Thus, the active Raman modes lead to the polarizability enhancement of the AA making them active and potent NLO materials.

3.6 UV–Vis spectral analysis

To understand the electronic transitions of the AA, the UV–Vis absorption peak is computed (Fig. 6). The electronic absorption spectra were calculated using time dependent-DFT method (TD-DFT) based on B3LYP/6–311++G(d,p) level optimization. The obtained spectra provide information about the vertical excitation energies (E), oscillator strengths (f), and the wavelength (λ) at which the transitions occur. A broad and strong absorption band was recorded for almost all the AA in range 200–300 nm range (Fig. 6(a)), except **Tryptophan** and **Threonine** for which the spectra range between 200-350 nm and 185–275 nm respectively. The π-π* and n-π* electronic transitions occurring at the highest wavelengths are represented by transitions $S_0 \rightarrow S_1$, S_2, and S_3 (SD 3). **Histidine, Lysine, Phenylalanine**, and **Tryptophan** has the highly intense absorbance spectra with absorbance intensity of about 1400, 900, 2000, and 3000 AU. For **Histidine, Lysine**, and **Tryptophan**, transition $S_0 \rightarrow S_2$ existing with excitation energy of 4.85, 5.23, and 4.56 eV were responsible for the peak formation in the spectra. **Phenylalanine** has $S_0 \rightarrow S_2$ transition majorly contributing in the formation of peak. $S_0 \rightarrow S_2$ has highest excitation energy of 5.37 eV. **Leucine, Methionine, Threonine**, and **Valine** have the absorption spectra with intermediate value of intensity of 600, 550, 350, and 450 AU. **Leucine**, **Methionine**, and **Threonine** has $S_0 \rightarrow S_2$ transition majorly contributing in the formation of absorption peak. The excitation energy of $S_0 \rightarrow S_2$ transition of **Leucine, Methionine**, and **Threonine** are 5.5, 5.01, and 5.65 eV respectively. **Threonine** has the highest value of excitation energy among all the other AA. **Isoleucine** has the smallest value of intensity (100 AU) for the absorbance peak. The excitation energies of electronic transitions for the AA are relatively close to the values of ΔE obtained from FMO analysis of the respective AA. These transitions show the enhanced intramolecular interactions between the lone pair (n) electrons and the π electron and also impart in molecule's unsaturation (Fleck and Petrosyan 2010). Thus, it can be said that the AA is highly reactive. Moreover, the $S_0 \rightarrow S_1$ transition for **Histidine** and **Tryptophan** AA has the highest wavelengths compared to the transitions of other AA. Thus, **Histidine** and **Tryptophan** can be considered more chemically reactive.

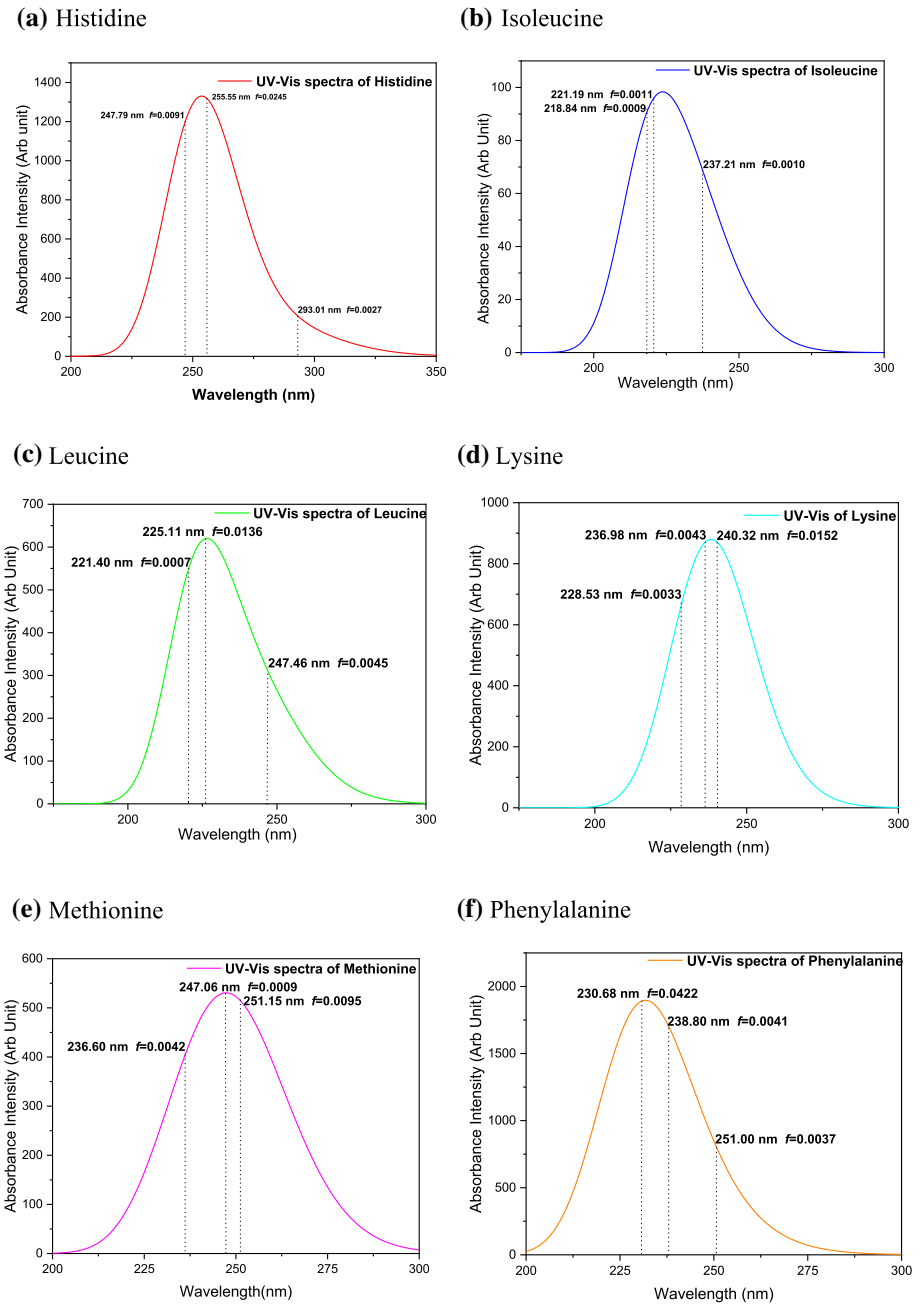

Fig. 6 Computational UV–Vis spectra of AA showing oscillator strength for three highest peaks of absorption bands

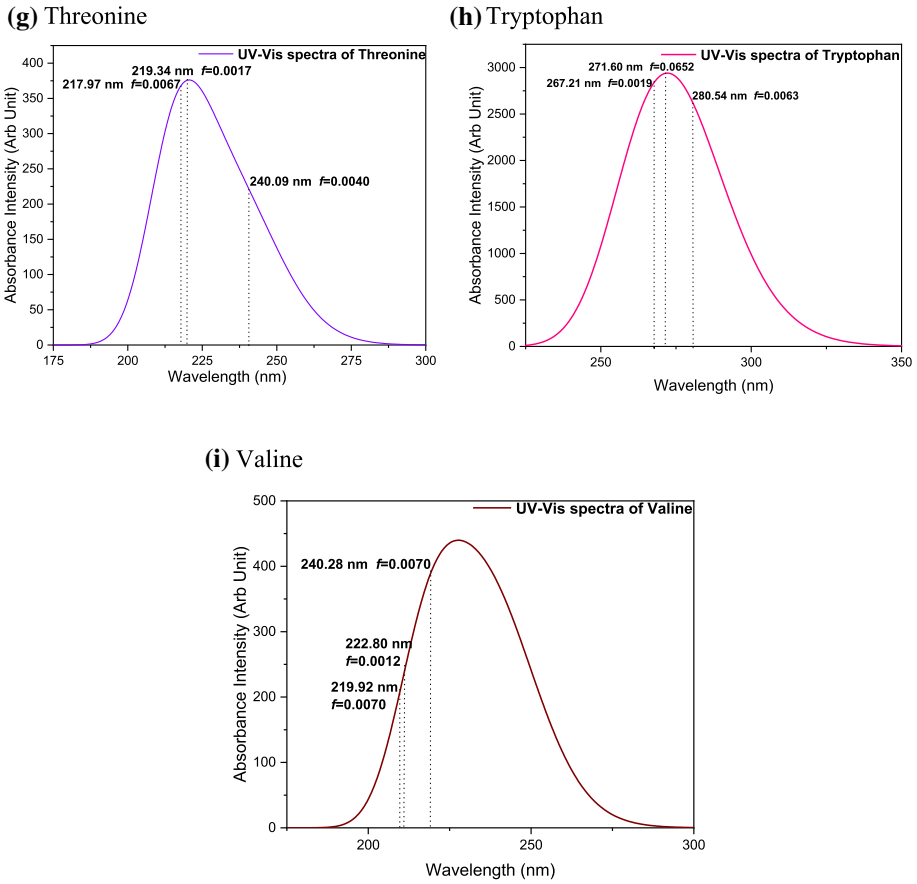

Fig. 6 (continued)

3.7 Linear and nonlinear optical analysis

Theoretical NLO calculation is most important part in identifying a potential NLO active molecule. The characterization of the behavior of the material in the presence of an applied electric field is accounted by phenomenon of polarization (Rana et al. 2018). Polarization simply tells us about the correlation between the interaction between the electron and nucleus. The multi-atom systems, such as molecules with large number of atoms have high number of electrons available as a charge cloud. The large the charge cloud is, the larger will be the possibility of charge dislocation. The highly raised values of the polarizability parameters are the result of the charge displacement. The literature survey revealed high optical nonlinearity among many organic and semi organic NLO materials. Thus, it is assumed that the materials having higher optical nonlinearity must be highly NLO active. The μ_{total}, α_{totab}, $\Delta\alpha$ and β_{total} is computed for all the EAA and is listed in Table 5. These parameters are basically expressed as the coefficients of standard Taylor series expansion of energy when the material interacts with weak and homogeneous externally applied electric field. Dipole moment is the first parameter in the list of polar properties as it accounts the polar nature of the molecule. The value of μ_{total}

Table 5 Computed values of total dipole moment (μ_{total}), total isotropic polarizability (α_{total}), anisotropy of polarizability ($\Delta\alpha$), and first order hyperpolarizability (β_{total}) of AA (dipole moment in Debye and μ_{total}, α_{totab}, $\Delta\alpha$ and β_{total} in esu)

AA	μ	α_{total}	$\Delta\alpha$	β
Histidine	5.13	14.78×10^{-24}	26.77×10^{-24}	1.99×10^{-30}
Isoleucine	1.21	13.10×10^{-24}	21.53×10^{-24}	1.23×10^{-30}
Leucine	2.01	13.19×10^{-24}	18.14×10^{-24}	1.4×10^{-30}
Lysine	1.1	14.9×10^{-24}	27.35×10^{-24}	2.06×10^{-30}
Methionine	1.69	14.5×10^{-24}	27.07×10^{-24}	1.37×10^{-30}
Phenylalanine	1.72	10.35×10^{-24}	32.23×10^{-24}	3.11×10^{-30}
Threonine	3.12	22.37×10^{-24}	15.56×10^{-24}	0.94×10^{-30}
Tryptophan	1.16	9.46×10^{-24}	14.58×10^{-24}	1.85×10^{-30}
Valine	1.44	11.46×10^{-24}	17.68×10^{-24}	1.75×10^{-30}

for AA are **Histidine** (5.13 Debye), **Isoleucine** (1.21 Debye), **Leucine** (2.01 Debye), **Lysine** (1.1 Debye), **Methionine** (1.69 Debye), **Phenylalanine** (1.72 Debye), **Threonine** (3.12 Debye), **Tryptophan** (1.16 Debye), and **Valine** (1.44 Debye). The electronic communication between acceptor and donor groups leads to high ICT. This results in the high values of polarizability and hyperpolarizability of the molecule. Thus, the transfer of the electron cloud from donor group towards acceptor group leads to the high value of the β_{total}. The first order hyperpolarizability has been computed using finite field theory approach (Kirtman et al. 1998). The computed values of α_{total} are **Histidine** (14.78×10^{-24}esu), **Isoleucine** (13.1×10^{-24}esu), **Leucine** (13.19×10^{-24}esu), **Lysine** (14.9×10^{-24}esu), **Methionine** (14.5×10^{-24}esu), **Phenylalanine** (10.35×10^{-24}esu), **Threonine** (22.37×10^{-24}esu), **Tryptophan** (9.46×10^{-24}esu), and **Valine** (11.46×10^{-24}esu). All these values are higher than α_{total} of Urea (5.66×10^{-24}esu). Among all the AA, **Threonine** has the highest value of α_{total}. It was four times higher than α_{total} of Urea. The computed values of $\Delta\alpha$ are **Histidine** (26.77×10^{-24}esu), **Isoleucine** (21.53×10^{-24}esu), **Leucine** (18.14×10^{-24}esu), **Lysine** (27.35×10^{-24}esu), **Methionine** (27.07×10^{-24}esu), **Phenylalanine** (32.23×10^{-24}esu), **Threonine** (15.56×10^{-24}esu), **Tryptophan** (14.58×10^{-24}esu), and **Valine** (17.68×10^{-24}esu). These values are also higher than $\Delta\alpha$ of Urea (6.30×10^{-24}esu). Again, the $\Delta\alpha$ of **Threonine** was found five times higher than $\Delta\alpha$ of Urea. The value of β_{total} for **Histidine** (1.92×10^{-30} esu), **Isoleucine** (1.23×10^{-30} esu), **Leucine** (1.4×10^{-30}esu), **Lysine** (2.06×10^{-30} esu), **Methionine** (1.37×10^{-30} esu), **Phenylalanine** (3.11×10^{-30} esu), **Threonine** (0.94×10^{-30} esu), **Tryptophan** (1.85×10^{-30} esu), and **Valine** (1.75×10^{-30} esu) is higher than β_{total} of Urea (0.78×10^{-30} esu). But the value of β_{total} of **Phenylalanine** is approximately four times higher than that of Urea. For the validation of the results, the β_{total} of the **Phenylalanine** is also compared with some such NLO materials that have already been worked on and gave better results. The β_{total} of **Phenylalanine** is also found two and a half times higher than β_{total} of Phenyl urea (2.04×10^{-30} esu) (Marappan et al. 2019) and approximately one and a half times higher than β_{total} of 3-nitroaniline (1.34×10^{-30} esu) (Krishnakumar and Nagalakshmi 2008). So, it simply suggests that **Phenylalanine** has the highest magnitude of the NLO parameters among all the AA. Thus, the comparative study shows that **Phenylalanine** have the high capability to act as a potent NLO responsive molecule.

4 Conclusion

In the presented work, the comparison of optoelectronic and quantum chemical features have been performed for all the EAA. This was done with the help of ground state structure optimization and TD-DFT calculations. The variation in the bond lengths and bond angles of the AA presented that the regions near the functional groups present in the respective AA is the region with high chances of being chemically reactive. The Mulliken charge analysis is done to see the actual charge transfer among the AA. The variation in the charge between the amino and carboxyl group highlighted these regions as the most reactive regions. The global reactivity parameters and MEP surfaces also verified the reactivity of the AA. The π-π* and n-π* electronic transitions are found to be occurring at highest wavelengths in computed absorption spectra. High Raman intensity modes are obtained for the AA from computed vibrational spectra. The Raman modes and electronic transitions obtained in the spectra validates the high polarizability of the AA molecules. For validating the high polarizability of the AA, the polarizability parameters (μ_{total}, α_{total}, $\Delta\alpha$ and β_{total}) were computed. The β_{total} of **Phenylalanine** was found higher than all the other AA and reference materials Urea, Phenyl urea and 3-nitroaniline. The comparison was sufficiently high enough to validate the NLO candidature of **Phenylalanine**. By this study, we can conclude that **Phenylalanine** is the most active EAA among all the others and it can be used for experimental validations in future. There is a strong possibility to use it in NLO applications.

Supplementary Information The online version contains supplementary material available at https://doi.org/10.1007/s11082-022-04118-4.

Author's contribution SL: Data curation, Writing-Original draft preparation, Visualization, Investigation, Software, Validation. MR: Conceptualization, Methodology, Writing-Reviewing and Editing, Supervision. KD: Conceptualization, Writing- Reviewing and Editing.

Data Availability Structure: https://pubchem.ncbi.nlm.nih.gov/, Extension conversion: http://openbabel.org/wiki/Main_Page, Optimization: https://gaussian.com/, Data analysis: https://gaussian.com/gaussview6/, Graph plotting: https://www.originlab.com/

Declarations

Conflict of interest The authors declare that they have no known competing financial interests or personal relationships that could have appeared to influence the work reported in this paper.

References

Akinyele, O.F., Adekunle, A.S., Olayanju, D.S., Oyeneyin, O.E., Durodola, S.S., Ojo, N.D., Aanuoluwapo, A.A., Ajayeoba, T.A., Olasunkanmi, L.O.: Synthesis and corrosion inhibition studies of (E)-3-(2-(4-chloro-2-nitrophenyl)diazenyl)-1-nitrosonaphthalen-2-ol on mild steel dissolution in 0.5 M HCl solution- experimental DFT and monte carlo simulations. J. Mol. Struct. **1268**, 133738 (2022). https://doi.org/10.1016/j.molstruc.2022.133738

Bairy, R., Jayarama, A., Kulkarni, S.D., Murari, M.S., Vijeth, H.: Improved nonlinear optical absorption mechanism and susceptibility (Ï(3)) of CdS nanostructured thin films: role of zinc doping. Mater Sci Semicond Process. **121**, 105400 (2021). https://doi.org/10.1016/j.mssp.2020.105400

Becke, A.D.: Density-functional thermochemistry III The role of exact exchange. J. Chem. Phys. **98**, 5648 (1993). https://doi.org/10.1063/1.464913

Becke, A.D.: Density-functional thermochemistry. V. Systematic optimization of exchange-correlation functionals. J. Chem. Phys. **107**, 8554–8560 (1997). https://doi.org/10.1063/1.475007

Bhatt, H., Pant, T., Dhoundiyal, C.C., Rana, M., Chowdhury, P., Joshi, P.C., Arya, P., Tiwari, H.: Computational study of the intermolecular interactions and their effect on the UV-visible spectra of the ternary liquid mixture of benzene, ethanol and propylene glycol. J Mol Model. **26**, 268 (2020). https://doi.org/10.1007/s00894-020-04533-y

Buriahi, A., Singh, M.S., Arslan, V.P.: Gamma-ray attenuation properties of some NLO materials: potential use in dosimetry. Radiat Environ Biophys. **59**, 145–150 (2020). https://doi.org/10.1007/s00411-019-00824-y

Cheng, Q., Shi, X., Li, C., Jiang, Y., Shi, Z., Zou, J., Wang, X., Wang, X., Cui, Z.: Chromophores with side isolate groups and applications in improving the poling efficiency of second non-linear optical (NLO) materials. Dyes Pigm. **162**, 721–727 (2019). https://doi.org/10.1016/j.dyepig.2018.11.001

Christophersen, O.A., Haug, A.: Animal products diseases and drugs: a plea for better integration between agricultural sciences human nutrition and human pharmacology. Lipids Health Dis. (2011). https://doi.org/10.1186/1476-511X-10-16

Dennington, R., Keith, T., Millam, J.: GaussView Version 412. Semichem, Inc., Shawnee Mission, KS (2007).

Fleck, M., Petrosyan, A.M.: Difficulties in the growth and characterization of non-linear optical materials: a case study of salts of amino acids. J. Cryst. Growth. **312**, 2284–2290 (2010). https://doi.org/10.1016/j.jcrysgro.2010.04.054

Frisch, M. J., Trucks, G. W., Schlegel, H. B. et al.: Gaussian 09, Revision B. 01, Gaussian Inc., Wallingford CT. **121**, 150–166 (2009).

Huang, X., Braams, B.J., Bowman, J.M.: Ab initio potential energy and dipole moment surfaces of $(H_2O)_2$. J. Phys. Chem. a. **110**, 445–451 (2006). https://doi.org/10.1021/jp053583d

Idouhli, R., Ousidi, A.N., Khadiri, M.E., Abouelfida, A., Itto, M.Y.A., Auhmani, A., Benyaich, A.: Electrochemical and theoretical studies of some monoterpenic thiazolidinones as corrosion inhibitors for steel in acidic media. J Adhes Sci Technol. **35**, 1404–1425 (2021). https://doi.org/10.1080/01694243.2020.1850011

Javier-Hila, A.M.V., Javier, B.C.V., Hila, F.C., Guillermo, N.R.D.: Photon attenuation parameters of non-essential amino acids using EPICS2017 library interpolations. SN Appl. Sci. **3**, 542 (2021). https://doi.org/10.1007/s42452-021-04507-6

John, N.L., Abraham, S., Sajan, D., Philip, R., Joy, N., Chitra, R.: Molecular structure, NLO properties and vibrational analysis of l-Histidine tetra fluro borate by experimental and computational spectroscopic techniques. Spectrochim. Acta A Mol. Biomol. Spectrosc. **226**, 117615 (2020). https://doi.org/10.1016/j.saa.2019.117615

Khnifira, M., Hamidi, S.E., Mahsoune, A., Sadiq, M., SerdaroÄŸlu, G., Kaya, S., Qourzal, S., Barka, N., Abdennouri, M.: Adsorption of methylene blue cationic dye onto brookite and rutile phases of titanium dioxide: quantum chemical and molecular dynamic simulation studies. Inorg. Chem. Commun. **129**, 108659 (2021). https://doi.org/10.1016/j.inoche.2021.108659

King, T.A., Kandemir, J.M., Walsh, S.J., David, R.: Photocatalytic methods for amino acid modification. Chem. Soc. Rev. Spring. **50**(1), 39–57 (2021). https://doi.org/10.1039/D0CS00344A

Kirtman, B., Luis, J.M., Bishop, D.M.: Simple finite field method for calculation of static and dynamic vibrational hyperpolarizabilities: curvature contributions. J. Chem. Phys. **108**, 10008 (1998). https://doi.org/10.1063/1.476460

Koopmans, T.: About the assignment of wave functions and eigenvalues for the individual electrons in an atom. Physica. **1**, 104–113 (1934). https://doi.org/10.1016/S0031-8914(34)90011-2

Krishnakumar, V., Nagalakshmi, R.: Studies on the first-order hyperpolarizability and terahertz generation in 3-nitroaniline. Phys. b: Condens. Matter. **403**, 1863–1869 (2008). https://doi.org/10.1016/j.physb.2007.10.341

Kuramochi, H., Aoyama, G., Okajima, H., Sakamoto, A., Kanegawa, S., Sato, O., Takeuchi, S., Tahara, T.: Femtosecond polarization switching in the crystal of a [CrCo] dinuclear complex. Angew. Chem. **132**, 15999–16003 (2020). https://doi.org/10.1002/ange.202004583

Lakhera, S., Devlal, K., Ghosh, A., Rana, M..: In silico investigation of phytoconstituents of medicinal herb piper longum against SARS-CoV-2 by molecular docking and molecular dynamics analysis. Res. Chem. (2021). https://doi.org/10.1016/j.rechem.2021.100199

Lakhera, S., Devlal, K., Ghosh, A., Rana, M.: Modelling the DFT structural and reactivity study of feverfew and evaluation of its potential antiviral activity against COVID-19 using molecular docking and MD simulations. Chem. Pap. (2022a). https://doi.org/10.1007/s11696-022-02067-6

Lakhera, S., Rana, M., Devlal, K., Yadav, R., Celik, I.: A comprehensive exploration of pharmacological properties, bioactivities and inhibitory potentiality of luteolin from Tridax procumbens as anticancer drug by in-silico approach. Struct Chem (2022b). https://doi.org/10.1007/s11224-022-01882-7

Lakhera, S., Devlal, K., Rana, M., Dhuliya, V.: Quantum mechanical study of three aromatic bioactive fatty alcohol compounds with nonlinear optical and potential light harvesting properties. Opt. Mater. **129**, 112476 (2022c). https://doi.org/10.1016/j.optmat.2022.112476

Lakhera, S., Devlal, K., Rana, M., Celik, I.: Study of nonlinear optical responses of phytochemicals of Clitoria ternatea by quantum mechanical approach and investigation of their anti-Alzheimer activity with in silico approach. Struct Chem (2022d). https://doi.org/10.1007/s11224-022-01981-5

Lee, S.T., Khairul, W.M., Lee, O.J., Rahamathullah, R., Daud, A.I., Halim, K., Bulat, K., Sapari, S., Razak, F.I.A., Krishnan, G.: Electronic, reactivity and third order nonlinear optical properties of thermally-stable push-pull chalcones for optoelectronic interest: experimental and DFT assessments. J. Phys. Chem. Solids. **159**, 110276 (2021). https://doi.org/10.1016/j.jpcs.2021.110276

Lopez, M. J., Mohiuddin, S. S.: Biochemistry. Essential Amino Acids. (2022). https://www.ncbi.nlm.nih.gov/books/NBK557845/?report=classic

Marappan, D., Palanisamy, M., Shu, H.M., Balraj, B., Sivakumar, C.: Growth, vibrational, optical, mechanical and DFT investigations of an organic nonlinear optical material – phenylurea. Z. Phys. Chem. **233**, 1659–1682 (2019). https://doi.org/10.1515/zpch-2018-1230

Midgley, P., Dunin, P., Borkowski, R.: Electron tomography and holography in materials science. Nature Mater. **8**, 271–280 (2009). https://doi.org/10.1038/nmat2406

Moroz, L., Maslovskaya, A.: Fractional differential model of domain boundary kinetics in ferroelectrics. Comput Approach AIP Conference Proc. **2328**, 020001 (2021). https://doi.org/10.1063/5.0042140

Muhammad, S., Nakano, M.: Computational strategies for nonlinear optical properties of carbon nano-systems. Nanosci Comput Chem: Res Progress (2013). https://doi.org/10.1201/b16368-10

Muhammad, S., Nakano, M., Al-Sehemi, A.G., Kitagawa, Y., Irfan, A., Chaudhry, A.R., Kishi, R., Ito, S., Yoneda, K., Fukuda, K.: The role of singlet diradical character in carbon nanomaterials: a novel hot spot for efficient nonlinear optical materials. NANOHL (2016). https://doi.org/10.1039/C6NR06097H

Muhammad, S., Xu, H. L., Zhong, R. L., Su, Z. M., Al Sehemic, A. G.: A. Irfan, Quantum chemical design of nonlinear optical materials by sp2 -hybridized carbon nanomaterials: issues and opportunities. J. Mater. Chem. C. **1,** 5439–5449 (2013). https://doi.org/10.1039/c3tc31183j.

Naseema, K., Sreedharan, R., Ravi, S., Raghi, K.R., Kumar, M.: Experimental and computational studies on optical properties of a promising N-benzylideneaniline derivative for non-linear optical applications. Z. Naturforsch. **75**, 557–573 (2020). https://doi.org/10.1515/zna-2020-0047

Nazrin, S.N., Halimah, M.K., Muhammad, F.D.: Comparison study of optical properties on erbium-doped and silver-doped zinc tellurite glass system for non-linear application. J. Mater. Sci: Mater. Electron. **30**, 6378–6389 (2019). https://doi.org/10.1007/s10854-019-00940-x

Ojo, N.D., Krause, R.W., Egbedi, N.O.O.: Electronic and nonlinear optical properties of 2-(((5-aminonaphthalen-1-yl)imino)methyl)phenol: experimental and time-dependent density functional studies. J. Mol. Liq. **319**, 114157 (2020). https://doi.org/10.1016/j.molliq.2020.114157

Oyeneyin, O.E., Ojo, N.D., Ipinloju, N., James, A.C., Agbaffa, E.B.: Investigation of corrosion inhibition potentials of some aminopyridine schiff bases using density functional theory and monte carlo simulation. Chemistry Africa **5**, 319–332 (2022). https://doi.org/10.1007/s42250-021-00304-1

Pathade, S., Jagdale, B.: Experimental and computational investigations on the molecular structure vibrational spectra electronic properties FMO and MEP analyses of 46-Bis(4-Fluorophenyl)-56-dihydropyrimidin-2(1H)-one: A DFT Insight. Phys. Chem. Res. (2020). https://doi.org/10.22036/pcr.2020.227546.1763.

Prettre, G., Pullman, G.: Quantum mechanical calculations of NMR chemical shifts in nucleic acids. Q. Rev. Biophys. **20**, 113–172 (1987). https://doi.org/10.1017/S0033583500004169

Rana, M., Chowdhury, P.: Nonlinear optical responses of organic based indole derivative: an experimental and computational study. Mater. Today: Proc. **28**(1), 241–245 (2020). https://doi.org/10.1016/j.matpr.2020.01.598

Rana, M., Singla, N., Chatterjee, A., Shukla, A., Chowdhury, P.: Investigation of nonlinear optical (NLO) properties by charge transfer contributions of amine functionalized tetraphenylethylene. Opt. Mater. **62**, 80–89 (2016). https://doi.org/10.1016/j.optmat.2016.09.043

Rana, M., Singla, N., Pathak, A., Dhanya, A., Narayana, C., Chowdhury, P.: Vibrational-electronic properties of intra/inter molecular hydrogen bonded heterocyclic dimer: an experimental and theoretical study of pyrrole-2-carboxaldehyde. Vib. Spectrosc. **89**, 16–25 (2017). https://doi.org/10.1016/j.vibspec.2016.12.003

Rana, M., Chatterjee, A., Chowdhury, P.: Investigation of nonlinear optical properties of organic based di amine substituted tetraphenylethylene. AIP Conf. Proc. **2009**, 020055 (2018). https://doi.org/10.1063/1.5052124

Rana, M., Jain, A., Rani, V., Chowdhury, P.: Glutathione capped core/shell CdSeS/ZnS quantum dots as a medical imaging tool for cancer cells. Inorg. Chem. Commun. **112**, 107723 (2020). https://doi.org/10.1016/j.inoche.2019.107723

Rana, M., Pooja, Chowdhury, P., Investigation on nonlinear optical responses of different pyrrole derivatives: a computational study. AIP Conf. Proc. (2019). https://doi.org/10.1063/1.5120919.

Ray, P.C.: Size and shape dependent second order nonlinear optical properties of nanomaterials and their applications in biological and chemical sensing. Chem. Rev **110**, 5332–5365 (2010). https://doi.org/10.1021/cr900335q

Saito, K., Mitsuhashi, K., Ishikita, H.: Dependence of the chlorophyll wavelength on the orientation of a charged group: why does the accessory chlorophyll have a low site energy in photosystem II? J. Photochem. Photobiol. **402**, 112799 (2020). https://doi.org/10.1016/j.jphotochem.2020.112799

Senthilkumar, S., Seralathan, J., Muthukumaran, G.: Synthesis, structure analysis, biological activity and molecular docking studies of some hydrazones derived from 4-aminobenzohydrazide. J. Mol. Struct. **1226**, 129354 (2021). https://doi.org/10.1016/j.molstruc.2020.129354

Sheikhi, M., Shahab, S., Alnajjar, R., Ahmadianarog, M.: Adsorption properties of the new anti-cancer drug alectinib on CNT (6,6–6) nanotube: geometry optimization, molecular structure, spectroscopic (NMR, UV/Vis, Excited State), FMO, MEP and HOMO–LUMO investigations. J Clust Sci. **30**, 83–96 (2019). https://doi.org/10.1007/s10876-018-1460-9

Soares, J.D.P., Scott, H.L., Teixeira, F.J., Gustavo, P.D.: Dietary amino acids and immunonutrition supplementation in cancer-induced skeletal muscle mass depletion: a mini-review curr. Pharm. Des. **26**, 970–978 (2020). https://doi.org/10.2174/1381612826666200218100420

Swartling, D. J., Coonce, J. G., Cashman, D. J.: Using balloons to model pi-conjugated systems and to teach frontier molecular orbital theory. World J. Chem. Educ. **6**, 102–106 (2018). https://doi.org/10.12691/wjce-6-2-5.

Then, A., Mácha, K., Ibrahim, B.: A novel method for achieving an optimal classification of the proteinogenic amino acids. Sci Rep. **10**, 15321 (2020). https://doi.org/10.1038/s41598-020-72174-5

Ullah, F., Kosar, N., Ali, A., Maria, Mahmood, T., Ayub, K.: Alkaline earth metal decorated phosphide nanoclusters for potential applications as high performance NLO materials: a first principle study. Phys. E: Low-Dimens. Syst. Nanostructures. (2020). https://doi.org/10.1016/j.physe.2019.113906.

Visscher, K.M., Geerke, D.P.: Deriving Force-field parameters from first principles using a polarizable and higher order dispersion model. J. Chem. Theory Comput. **15**, 1875–1883 (2019). https://doi.org/10.1021/acs.jctc.8b01105

Wang, H., Xi, Q., Liang, P., Zheng, L., Hong, Y., Zuo, Y.: IHEC_RAAC: an online platform for identifying human enzyme classes via reduced amino acid cluster strategy. Amino Acids **53**, 239–251 (2021). https://doi.org/10.1007/s00726-021-02941-9

Authors and Affiliations

Shradha Lakhera[1] · Meenakshi Rana[1] · Kamal Devlal[1]

✉ Meenakshi Rana
mrana@uou.ac.in

[1] Department of Physics, School of Sciences, Uttarakhand Open University, Haldwani, Uttarakhand 263139, India